Inorganic Chemistry

Article

pubs.acs.org/IC

Metal-Assisted Ring-Closing/Opening Process of a Chiral Tetrahydroquinazoline

Ana M. García-Deibe,[†] Jesús Sanmartín-Matalobos,*[,†] Concepción González-Bello,[‡] Emilio Lence,[‡] Cristina Portela-García,[†] Luis Martínez-Rodríguez,[†] and Matilde Fondo[†]

[†]Departamento de Química Inorgánica, Facultad de Química, Universidad de Santiago de Compostela, 15782 Santiago de Compostela, Spain

[‡]Centro Singular de Investigación en Química Biológica y Materiales Moleculares (CIQUS), Universidad de Santiago de Compostela, 15782 Santiago de Compostela, Spain

Supporting Information

ABSTRACT: The ring−chain tautomerism of a 2-aryl-1,2,3,4-tetrahydroquinazoline has been exploited to induce reversible changes in the aminal−imine equilibrium, as desired, by coordination of a suitable metal ion. This process was studied by NMR and UV−vis spectroscopies, X-ray crystallography, and molecular modeling approach. The results obtained show that the imine H_2L^i undergoes a selective ring-closing reaction upon complexation with Ni^{2+}. As a result, complexes of the type $Ni(HL^a)_2$ are obtained, whose chirality arises from the chiral ligand H_2L^a and the helicity of the structure. Hence, helical enantiomers form the following racemates: [Δ-C(*R*,*R*)N(*S*,*S*),Λ-C(*S*,*S*)N(*R*,*R*)]-$Ni(HL^a)_2$·2HOAc and [Δ,Λ-C-(*S*,*R*)N(*R*,*S*)]-$Ni(HL^a)_2$·4MeOH. In contrast to the situation observed for Ni^{2+}, the cyclic tautomer of the ligand, H_2L^a, undergoes a selective ring-opening reaction upon complex formation with Pd^{2+}, ultimately yielding $Pd(HL^i)_2$·MeOH, in which the open-chain imine ligand is bidentate through the *N*,*O* donor set of the quinoline residue. Density functional theory calculations were conducted to provide insight into the different behavior of both coordinated metals (Ni^{2+} and Pd^{2+}) and to propose a mechanism for the metal-assisted opening/closing reaction of the tetrahydroquinazoline ring.

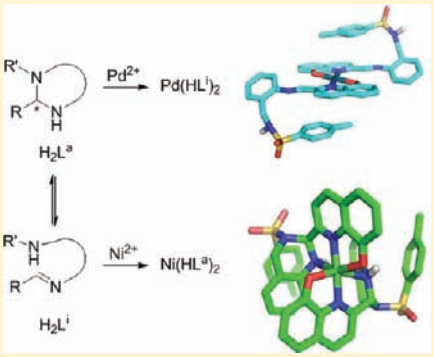

INTRODUCTION

Imines and related compounds that contain a carbon−nitrogen double bond are very attractive systems because they can easily undergo reversible reactions under certain conditions. For instance, imines can undergo *E*−*Z* isomerization reactions, nucleophilic additions, hydrolysis, transamination reactions, tautomerism, aza Diels−Alder reactions, etc. Among those, we became interested in a particular tautomerism that involves ring-closing/opening reactions by reversible cyclization of imines.[1−8]

In the absence of metal ions, the formation of imidazolidine,[1,6] benzimidazoline,[5] and hexahydropyrimidine[6] rings from adequate imines occurs, as a result of an intramolecular nucleophilic addition of the amino $N^{\delta-}$ atom to the electrophilic $C^{\delta+}$ center of the imine. As a result, the sp^2-hybridized imine carbon site becomes an sp^3-hybridized benzimidazoline, imidazolidine, and hexahydropyrimidine center, and no extra gain in the conjugation energy exists. Owing to the absence of the conjugation effect, the ring-opening is facilitated and readily observed upon complex formation with Fe^{3+}, Fe^{2+}, Ni^{2+}, Cu^{2+}, and Zn^{2+} ions depending on the aminal ring.

Boča et al.[1] have postulated that, in the presence of metal ions, the acidity of the attacking metal ion competes with the acidity of the −C═N− site, so that there is a balance between a $N^{\delta-}$ atom and $C^{\delta+}$ center coming together (imidazolidine ring-closing) and going apart (imidazolidine ring-opening). Which direction the system will go depends on the relative importance of the acidity of $C^{\delta+}$ and M^{n+} centers. Weak Lewis acids (such as Fe^{2+}, Co^{2+}, and Cu^{2+}) are incapable (or only partly capable) of opening the imidazolidine ring, whereas stronger Lewis acids (e.g., Fe^{3+} and Zn^{2+}) can readily do it. In contrast, Tuchagues et al.[6] conclude that the metal size plays a prominent role in shifting the ligand equilibrium toward the tautomeric form most appropriate to each specific cation. LS Fe^{2+} has a small enough size (75 pm) to stabilize the imine isomer in its complex, while the size of Ni^{2+} (83 pm) is probably too large for allowing coordination of the imine tautomer, and thus it stabilizes the imidazolidine tautomer.

Our interest in novel chiral ligands[7,9] led us to explore the reaction between 8-hydroxyquinoline-2-carboxaldehyde and *N*-(2-aminobenzyl)-4-methylbenzenesulfonamide in a 1:1 molar ratio, which could result in a chiral tetrahydroquinazoline H_2L^a or in an achiral imine H_2L^i (Scheme 1). We are also interested in investigating the factors influencing the ring-closing/opening process leading to H_2L^a or H_2L^i, and particularly whether metal coordination could be used to direct not only a ring-opening reaction, but also a ring-closing one. These processes involving

Received: May 24, 2011
Published: January 23, 2012

   dx.doi.org/10.1021/ic2017038 | *Inorg. Chem.* 2012, 51, 1278−1293

Scheme 1. Open-Chain Tautomer[a] H_2L^i en Route to the Final Thermodynamically Favored Aminal Ring Tautomer H_2L^a

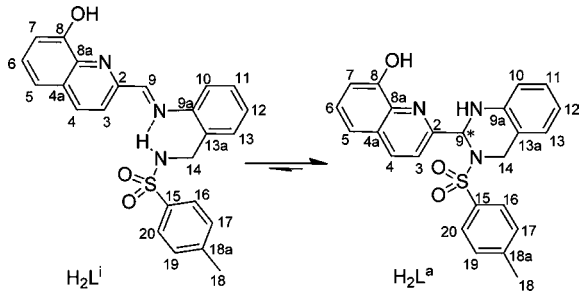

[a]The numbering scheme included was used for the assignment of the NMR signals, which is the same scheme used in the determination of the crystal structure for ease of understanding.

Ni^{2+} and Pd^{2+} ions have been studied by UV−vis and NMR spectroscopies as well as X-ray crystallography. Spectroscopic monitoring of the reactions here studied in conjunction with DFT calculations lead us to propose a mechanism for the closing/opening of the tetrahydroquinazoline ring.

RESULTS AND DISCUSSION

The design of imine H_2L^i for this study was based on the fine coordinating ability of the 8-hydroxyquinoline residue, which we have previously investigated,[10] as well as on the varied coordination alternatives offered by its aminal derivative H_2L^a (Scheme 1). The open-chain tautomer H_2L^i could provide up to four donor atoms (usually *O,N* bidentate and *O,N,N,N* tetradentate), whereas the cyclic tetrahydroquinazoline derivative can simultaneously coordinate a metal center with an *O,N,N* donor set at most. We selected for this study a borderline Lewis acid,[11] Ni^{2+} (η = 8.5 eV), and a soft Lewis acid, Pd^{2+} (η = 6.8 eV), that have been widely used to obtain octahedral[12] and square planar complexes,[13] respectively. It must be noted that the metal size of Ni^{2+} in an octahedral field (83 pm) is slightly larger than the Pd^{2+} one in a square planar field (78 pm).[14]

Free Ligand Ring-Opening/Closing. Condensation of the selectively functionalized *N*-(2-aminobenzyl)-4-methylbenzenesulfonamide[15] with 8-hydroxyquinoline-2-carboxaldehyde was spectroscopically monitored in order to understand the 6-*endo-trig* cyclization process (Scheme 2).[16] Tetrahydroquinazoline H_2L^a could result from the intramolecular nucleophilic addition of the sulfonamide *N* atom to the imine.[1,5,6]

It can be seen from Figure 1 that the imine H_2L^i is rapidly formed first, but already the presence of the chiral aminal H_2L^a is evident. The maximum imine/aminal ratio appears to be achieved after a period of about 1 h (ca. 4.5:1 ratio). After this time, the imine readily evolves to the tetrahydroquinazoline derivative, and only half an hour later an equimolar ratio is obtained. After a few hours the imine has virtually disappeared. A combination of bidimensional spectroscopic correlations (HMQC, HMBC, COSY, and NOESY) and NOE experiments enabled good identification of H_2L^i and H_2L^a in solution (see Supporting Information). These experiments were used to elucidate the possible conformations of H_2L^i and H_2L^a in solution, and sketches of the conformations are depicted in Scheme 1. Thus, on one hand, the observation of the inversion of imine H-9, enhancing exclusively H-10 (4.7%) and not H-3, indicates not only the typical *E* configuration of the imine

Scheme 2. Proposed Mechanism for the Formation of the Imine H_2L^i and 1,2,3,4-Tetrahydroquinazoline H_2L^a

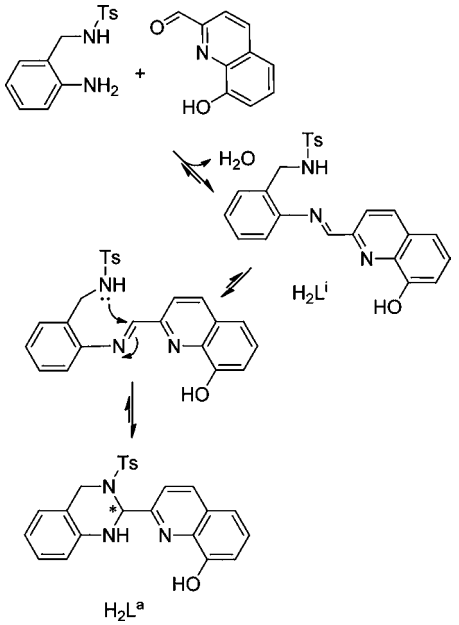

group, but that the four potential donor atoms of H_2L^i are *exo* orientated in two separate binding sites, *N,O* and *N,N*, as shown in Scheme 1. In this *exo* conformation, H_2L^i could be stabilized by an intramolecular N−H···N bond, the existence of which was deduced from the ν(N−H) and ν(C=N_{imine}) bands observed in the infrared spectrum. On the other hand, and in contrast to H_2L^i, cross-peaks between H_{ax}-14···H-3 and OH···NH show that the three potential donor atoms of H_2L^a can offer an *N,N,O* binding site.

In order to understand the thermodynamic preference of the cyclic compound H_2L^a relative to the open-chain one, H_2L^i, geometry optimizations and energy calculations in vacuum were performed using the Gaussian 09W[17] program package at density functional theory (DFT) level by means of the hybrid M06 functional[18,19] using the standard 6-31G(d) basis set. A polarizable continuum[20] solvation model (methanol as solvent) was also used for energy calculations to take into account the solvent effect, but similar trends were found both in vacuum and methanol (see Supporting Information). According to these calculations in methanol, the 1,2,3,4-tetrahydroquinazoline H_2L^a is 7.93 kcal mol^{-1} more stable than the most stable conformation of imine H_2L^i. This energy difference could be substantial enough to explain the total predominance of the cyclic compound over the open-chain imine form when the reaction time exceeds 4 h and 30 min. Moreover, the calculated ΔG value in methanol for the cyclization reaction of H_2L^i to give H_2L^a (see Supporting Information) is also energetically favorable (−5.66 kcal mol^{-1}).

Metal-Assisted Ring-Opening/Closing Reaction. First, the behavior of Pd^{2+} in the tetrahydroquinazoline/imine ring-opening/closing reaction was studied. Treatment of tetrahydroquinazoline H_2L^a or imine H_2L^i with $Pd(OAc)_2$ in methanol afforded a palladium complex that was identified as $Pd(HL^i)_2$ by a combination of bidimensional spectroscopic correlations (HMQC, HMBC, COSY, and NOESY). These studies led us to conclude that the coordinative environment of the Pd^{2+} ion is square planar and the imine behaves as monoanionic. The observation of the sulfonamide *NH* signal coupled to the

dx.doi.org/10.1021/ic2017038 | Inorg. Chem. 2012, 51, 1278−1293

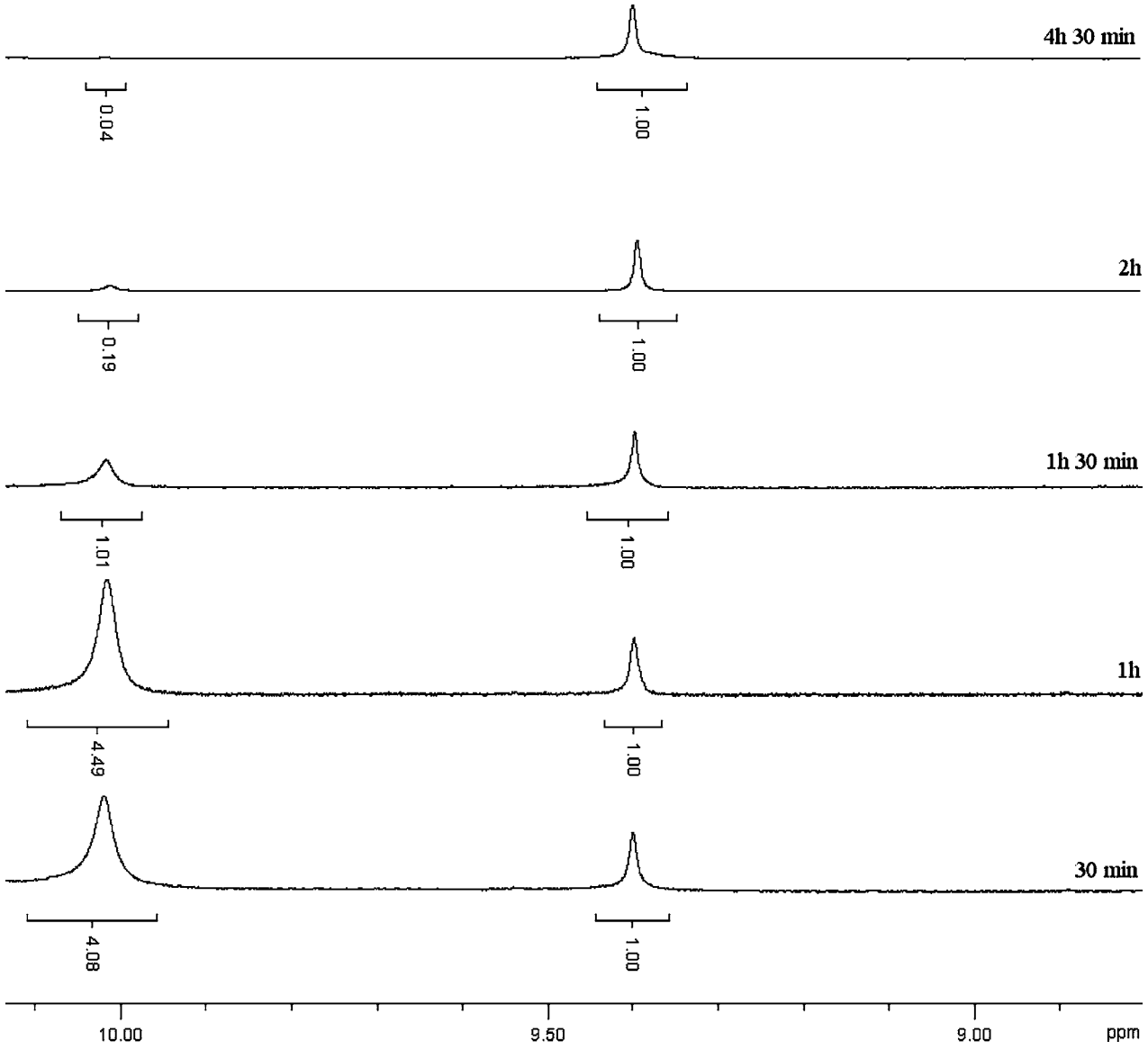

Figure 1. Sections of the ^{1}H NMR spectra in DMSO-d_6 corresponding to the successive samples of crude material extracted from the condensation reaction between *N*-(2-aminobenzyl)-4-methylbenzenesulfonamide and 8-hydroxyquinoline-2-carboxaldehyde. The signals at ca. 10 and 9.4 ppm correspond to phenolic protons of H_2L^i and H_2L^a, respectively. In all the spectra, integration values refer to the phenol signal of H_2L^i, which is considered as 1.00 for ease of comparison.

methylene protons demonstrates the monoanionic behavior of the ligand (see Supporting Information). As occurs in the free imine H_2L^i, the observed cross-peaks between protons H-10 and H-9 indicate that the four donor atoms are in two separate binding sites (*N,O* and *N,N*). NOESY cross-peaks due to alternative conformations were not detected. Moreover, the observed cross peaks between H-10 and H-7 indicate the close proximity of a benzylidene ring to a quinoline one.

The spectroscopic monitoring of the reaction between tetrahydroquinazoline H_2L^a and $Pd(OAc)_2$ in a 2:1 molar ratio (Figure 2) showed that $Pd(L^i)$ is rapidly formed first. In $Pd(L^i)$, which crystallized as $Pd(L^i)\cdot CH_2Cl_2$, the imine H_2L^i acts as an *O,N,N,N*-donor. During the first half hour of the reaction, there is no evidence for the formation of $Pd(HL^i)_2$. After this period, $Pd(L^i)$ gradually evolves into $Pd(HL^i)_2$ until it finally disappears. During the reaction, a substantial amount of cyclic ligand H_2L^a (without any evidence for H_2L^i) remains in solution, a situation that is due to the acidic media (pH about 5.5) caused by the acetic acid that arises from the formation of the metal complexes. After 2 h under reflux, $Pd(HL^i)_2$ could be isolated and subsequently characterized. It should be noted that a solution of $Pd(HL^i)_2$ under reflux readily yielded $Pd(L^i)$ and the tetrahydroquinazoline ligand H_2L^a, without any evidence for the formation of H_2L^i, thus showing the reversibility of the $Pd(L^i) + H_2L^a \leftrightarrow Pd(HL^i)_2$ equilibrium. In contrast, no evidence for reversibility was detected after 2 h under reflux at pH 5.5 for the process $H_2L^a + Pd^{2+} \rightarrow Pd(L^i)$.

In contrast to the results obtained for Pd^{2+}, the open-chain ligand H_2L^i, undergoes a selective ring-closing reaction upon complexation with Ni^{2+} in the crystallized octahedral complexes $Ni(HL^a)_2\cdot 4MeOH$ and $Ni(HL^a)_2\cdot 2HOAc$, in which the two units of the chiral cyclic ligand act as *O,N,N* tridentate donors. It should be noted that the formation of $Ni(HL^a)_2$ complexes did not depend on the ligand added, i.e., H_2L^i or H_2L^a. In fact, $Ni(HL^a)_2$ is quickly formed even on using imine H_2L^i as the starting free ligand.

dx.doi.org/10.1021/ic2017038 | *Inorg. Chem.* 2012, 51, 1278–1293

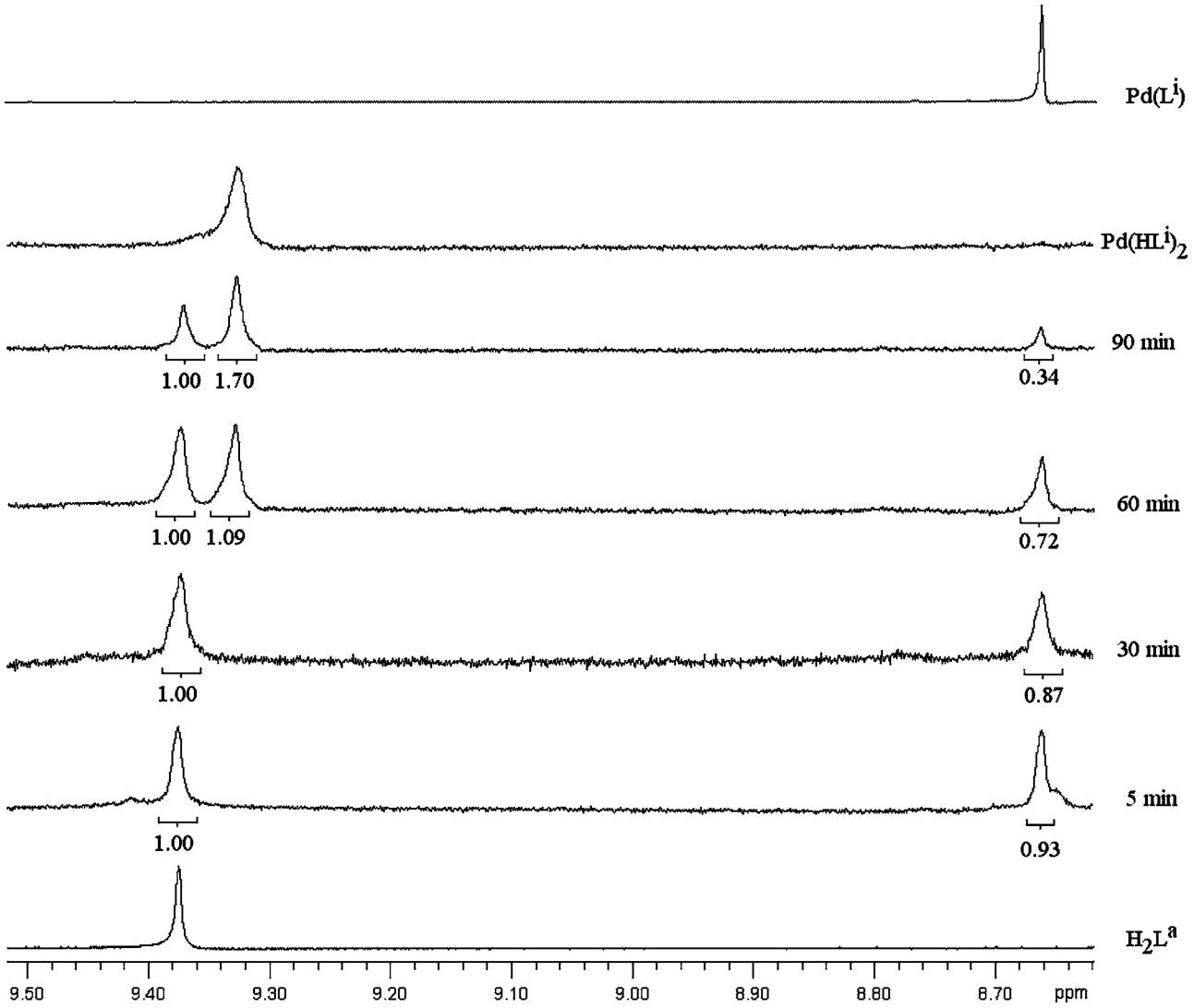

Figure 2. Sections of the ^{1}H NMR spectra in DMSO-d_6 corresponding to the successive samples of crude material extracted from the reaction under reflux of tetrahydroquinazoline H_2L^a and $Pd(OAc)_2$ in a 2:1 molar ratio. The azomethine signals around 9.33(s) and 8.66(s) ppm correspond to $Pd(HL^i)_2$ and $Pd(L^i)$, respectively. The integration value for the phenol signal of H_2L^a at 9.38(s) ppm was considered as 1.00 in all the spectra for ease of comparison.

The UV−vis absorption monitoring of the reaction at room temperature between H_2L^i and $Ni(OAc)_2{\cdot}4H_2O$ in a 1:1 molar ratio (Figure 3, top) shows that the reaction goes through the formation of $Ni(L^i){\cdot}MeOH$ en route to $Ni(HL^a)_2{\cdot}4MeOH$. Further evidence of the formation of $Ni(L^i){\cdot}MeOH$ was found in the infrared spectrum of the isolated compound that shows the characteristic $\nu(C{=}N_{imine})$ band and the absence of the $\nu(N{-}H)$ band (see Supporting Information). Figure 3, top, clearly shows that the absorbance of the characteristic band of $Ni(L^i){\cdot}MeOH$ (at about 304 nm) is decreasing gradually from start to finish. During 30 min of reaction the spectra show a decrease of the absorbance for the band at 248 nm that is accompanied by a considerable increase of absorbance for the band at 272 nm, which are signs that $Ni(HL^a)_2$ is forming and H_2L^i is consuming. Besides the mentioned bands that may be assigned to intraligand transitions, the electronic spectra exhibit two weak bands characteristic for the d−d transitions at about 380 nm (ν_3) and 510 nm (ν_2), as expected for six-coordinated octahedral nickel(II) complexes.[21] The monitoring of the reaction at room temperature between H_2L^a and $Ni(OAc)_2{\cdot}4H_2O$ in a 2:1 molar ratio (Figure 3, bottom) also shows the gradual formation of $Ni(HL^a)_2$, but in this case without any evidence for $Ni(L^i){\cdot}MeOH$.

Computational Studies: Proposed Mechanism. In order to gain some insight into the ring-opening/closing processes that the tautomers H_2L^a/H_2L^i undergo by complexation to Pd^{2+} and Ni^{2+} by forming $Pd(HL^i)_2$ and $Ni(HL^a)_2$, respectively, DFT calculations were performed, as described below.

The relative Gibbs free energy differences for the obtained $Pd(HL^i)_2$ versus other square planar Pd^{2+} complexes, i.e. $Pd(HL^a)(HL^i)$ and $Pd(HL^a)_2$, considering both possible enantiomers of H_2L^a (*R* or *S*) were first studied (Figure 4 and Supporting Information). Only a *trans* disposition of the coordinated ligands was considered, since a *cis* disposition appeared strongly disfavored in any case. Unexpectedly, these calculations predicted that $Pd(HL^a)_2$ complexes are the more stable ones, with little difference found between (*R*,*R*)- and (*R*,*S*)-stereoisomers (Figure 4). The difference in Gibbs free energy (ΔG) between the experimentally obtained complex

dx.doi.org/10.1021/ic2017038 | *Inorg. Chem.* 2012, 51, 1278−1293

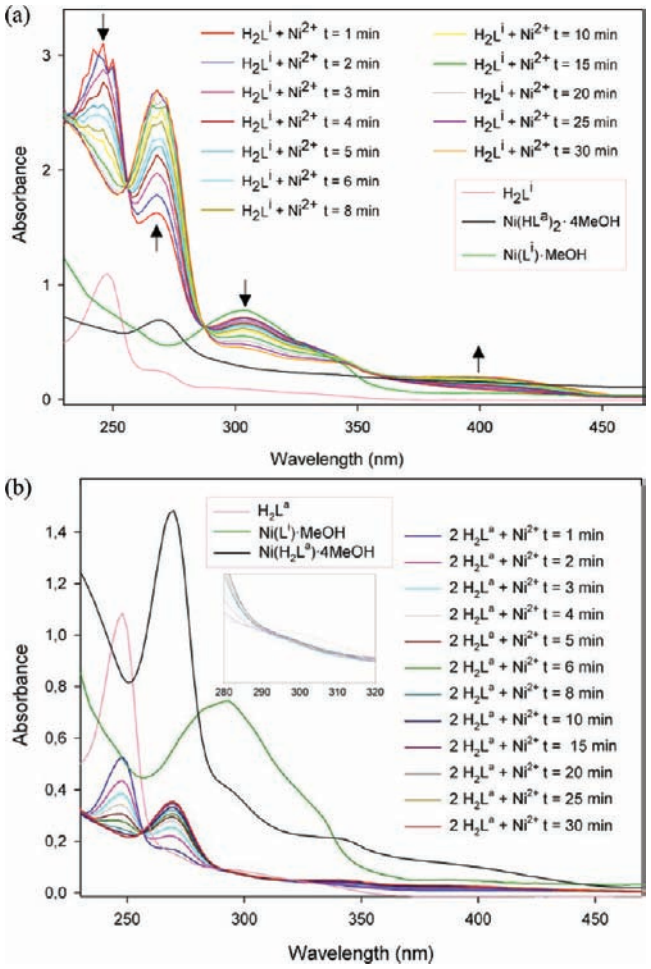

Figure 3. UV−vis spectroscopic monitoring of the reaction between H_2L^i/H_2L^a and $Ni(OAc)_2 \cdot 4H_2O$ (a) in 1:1 and (b) 2:1 molar ratios. Electronic spectra of H_2L^i/H_2L^a (pink line), $Ni(L^i) \cdot MeOH$ (green line), and $Ni(HL^a)_2 \cdot 4MeOH$ (black line) are included for comparison.

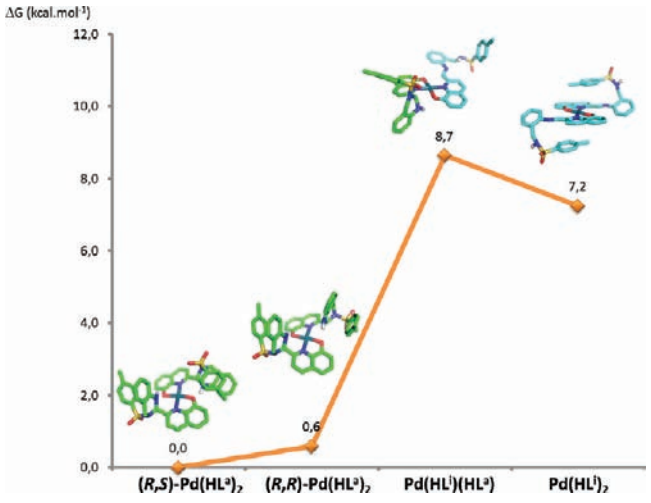

Figure 4. Relative Gibbs free energy for the most stable calculated conformers of (*R*,*S*)-$Pd(HL^a)_2$, (*R*,*R*)-$Pd(HL^a)_2$, $Pd(HL^i)(HL^a)$, and $Pd(HL^i)_2$ in methanol (left to right).

$Pd(HL^i)_2$ and the *R*,*S*-stereoisomer of $Pd(HL^a)_2$ (the most stable one) is 7.2 kcal mol^{-1}. Moreover, $Pd(HL^i)_2$ is 1.5 kcal mol^{-1} more stable than $Pd(HL^a)(HL^i)$.

The minimum energies for the most stable conformers of Ni^{2+} complexes with octahedral and square planar geometries have been calculated, before the calculation of the relative Gibbs free energy difference. The results indicate a clear preference for an octahedral geometry over a square planar one, with energy differences of over 19 kcal mol^{-1} (see Supporting Information). The relative Gibbs free energy difference for the most stable stereoisomers of octahedral $Ni(HL^a)_2$ complexes was calculated combining *R* and *S* enantiomers of the monodeprotonated cyclic ligand $(HL^a)^-$, as well as $Ni(HL^i)_2$ and $Ni(HL^a)(HL^i)$ (Figure 5). Among the possible octahedral

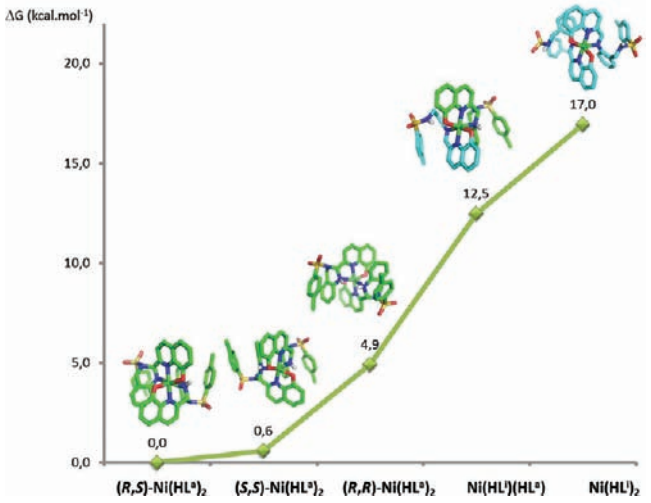

Figure 5. Relative Gibbs free energy for the most stable conformers calculated for octahedral nickel(II) complexes in methanol (from left to right): Λ-C(*S*,*R*)N(*R*,*S*)-$Ni(HL^a)_2$, Δ-C(*S*,*S*)N(*R*,*R*)-$Ni(HL^a)_2$, Δ-C(*R*,*R*)N(*S*,*S*)-$Ni(HL^a)_2$, $Ni(HL^a)(HL^i)$, and $Ni(HL^i)_2$ (see also Supporting Information for more details). In the figure only the chirality of the N donor atom has been indicated to simplify and reduce the size of the labels.

complexes, coordination to the *N,N,O* donor set provided by cyclic H_2L^a is clearly favored in comparison to that provided by H_2L^i (over 17 kcal mol^{-1}). The most stable species are both of the crystallized octahedral nickel(II) complexes, under the form of $Ni(HL^a)_2 \cdot 4MeOH$ and $Ni(HL^a)_2 \cdot 2HOAc$.

Spectroscopic monitoring of the reactions between H_2L^a/H_2L^i and Pd^{2+}/Ni^{2+} in 1:1 and 2:1 molar ratios gave important information that in conjunction with theoretical calculations have been considered to propose a mechanism for the closing/opening of the tetrahydroquinazoline ring. First, the final products are the same either using the open-chain ligand H_2L^i or the closed one H_2L^a. The remaining free ligand in solution is always the closed-chain ligand H_2L^a, with any evidence for H_2L^i. The use of a 1:1 molar ratio allows us to obtain complexes of the type $M(L^i)$ with both metal ions. Finally, the differences in the behaviors of both metals emerge when a 2:1 molar ratio is used, affording $Pd(HL^i)_2$ in one case and $Ni(HL^a)_2$ in the other. Moreover, during the reactions in 2:1 molar ratio, $Pd(L^i)$ was also observed en route to $Pd(HL^i)_2$, but any evidence for $Ni(L^i)$ en route to $Ni(HL^a)_2$ was found.

Given all the above, for a 1:1 molar ratio, the reaction would start with the formation of $M(L^i)$ that then evolves to $Pd(HL^i)_2$ or $Ni(HL^a)_2$. For a 2:1 molar ratio, when the metal is Pd^{2+}, the reaction pathway would be the same as for a 1:1 molar ratio, while for Ni^{2+} the formation of $Ni(HL^a)_2$ would follow an

dx.doi.org/10.1021/ic2017038 | Inorg. Chem. 2012, 51, 1278−1293

alternative path that will be discussed below. A plausible reaction mechanism is shown in Scheme 3. The key step of the

Scheme 3. General Proposed Mechanism for the Formation of Complexes of the Types $M(HL^i)_2$ and $M(HL^a)_2$

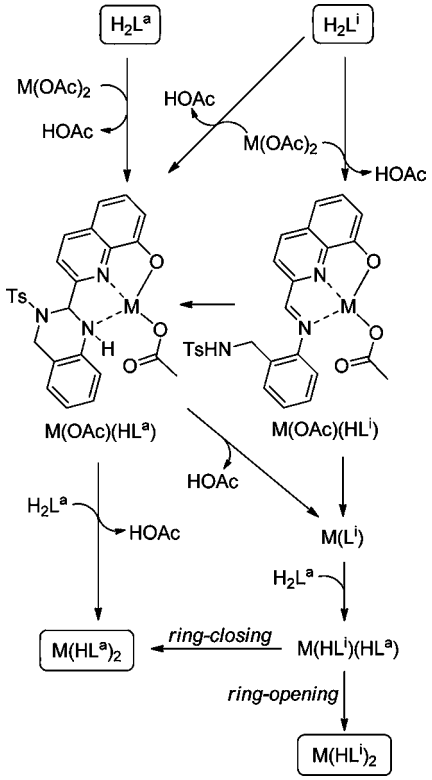

process would involve the intermediate complexes $M(HL^a)(HL^i)$ that could undergo an intramolecular ring-closing reaction to afford $Ni(HL^a)_2$ or an intramolecular ring-opening one to give $Pd(HL^i)_2$. The complete Gibbs free energy profile of the proposed pathway for both metals was analyzed, and the results are summarized in Figure 6.

The first step would involve the displacement of one of the acetate ligands in $M(OAc)_2$ by the open-chain ligand H_2L^i or the closed one H_2L^a to afford the square planar complexes $M(OAc)(HL^i)$ and $M(OAc)(HL^a)$, respectively. The displacement of the remaining acetate in $M(OAc)(HL^i)$ by the uncoordinated sulfonamide *N* atom of $(HL^i)^-$ leads to $M(L^i)$ complex. This process might be very fast considering the low Gibbs free energy involved (Figure 6). The conversion of $M(OAc)(HL^a)$ into $M(L^i)$ would involve a ring-opening reaction that will be initiated with the abstraction of the hydrogen atom of the aminal group by the acetate (Scheme 4). In $M(OAc)(HL^a)$ complexes, the coordination of the acetate ligand to the metal through one of the oxygen atoms locates the carbonyl group in an appropriate orientation for the intramolecular proton abstraction to give intermediate species of the type $M(HOAc)(L^a)$. Figure 7a,b shows the calculated transition states for the proton abstraction step. The calculated activation energy for the conversion of $M(OAc)(HL^a)$ into $M(HOAc)(L^a)$ is 5.28 kcal mol^{-1} when M = Pd^{2+} and 5.55 kcal mol^{-1} when M = Ni^{2+}. Therefore, the energy cost of the conversion of $M(OAc)(HL^a)$ into $M(L^i)$ basically corresponds to this hydrogen abstraction (Scheme 4). The next step would involve the ring-opening reaction with removal of acetic acid. The high energy required for the dissociation of acetic acid in $M(HOAc)(L^a)$ (10.85 kcal mol^{-1} for Pd^{2+} and 15.55 kcal mol^{-1} for Ni^{2+}) leads us to propose an associative mechanism. Attempts to calculate the activation energy involved in the subsequent ring-opening reaction and displacement of acetic acid failed because the intermediates rapidly evolve to the final $M(L^i)$ complexes, which is coherent with very low activation energies.

Once $M(L^i)$ complexes are formed, their coordination with the free closed-chain ligand in solution, H_2L^a, would afford the key intermediate complexes $M(HL^i)(HL^a)$. Examining the structure of the most stable conformer of both complexes, the octahedral $Ni(HL^i)(HL^a)$ (Figure 7c) and the square planar $Pd(HL^i)(HL^a)$ (Figure 7d) suggests that the different coordination of Ni^{2+} and Pd^{2+} in their complexes might be the key to the further evolution of these intermediate complexes. Figure 7c shows that in $Ni(HL^i)(HL^a)$ the imine moiety is coordinated to Ni^{2+} and the imine carbon atom is located at 3.0 Å from the sulfonamide *N* atom. So, this nitrogen is in the appropriate conformation to perform an intramolecular nucleophilic addition to the imine carbon atom, which is activated by the nickel ion. This agrees with the predicted energetically favorable conversion of $Ni(HL^i)(HL^a)$ into $Ni(HL^a)_2$, with a calculated ΔG of −12.48 kcal mol^{-1}. In contrast, such activation is not present in the square planar $Pd(HL^i)(HL^a)$ that displays an uncoordinated imine *N* atom (Figure 7d). In addition, the free lone pair of the sulfonamide *N* atom is rotated 180° against the imine carbon atom because the mentioned *N* atom establishes hydrogen bonding with the imine *N* atom in $Pd(HL^i)(HL^a)$. With this in mind, even though the conversion of $Pd(HL^i)(HL^a)$ into $Pd(HL^a)_2$ is energetically favorable, the activation energy for this process might be high. All attempts to locate a transition state with the free lone pair of the sulfonamide *N* atom close to Pd^{2+} failed, presumably due to steric crowding.

Considering that the reaction between H_2L^a and Pd^{2+} always goes via $Pd(L^i)$ regardless the molar ratio used, but any evidence for $Ni(L^i)$ en route to $Ni(HL^a)_2$ was found when a 2:1 molar ratio was used, an alternative pathway for the conversion of $Ni(OAc)(HL^a)$ into $Ni(HL^a)_2$ must be considered. This alternative process would involve the displacement of the acetate ligand in $Ni(OAc)(HL^a)$ by the closed-chain ligand H_2L^a (Scheme 4), which could be initiated by the abstraction of the phenol hydrogen atom in free H_2L^a by the acetate ligand in $Ni(OAc)(HL^a)$.

Crystal Structure of Tetrahydroquinazoline H_2L^a. Single crystal X-ray diffraction techniques confirmed that pale yellow prismatic crystals obtained after slow evaporation of a methanol solution of the condensed ligand consist of crystallographically independent molecules that comprise a 1,2,3,4-tetrahydroquinazoline ring. Table 1 shows the main bond distances and angles for H_2L^a that fall within the expected ranges.[22−24] In order to facilitate comparison, the equivalent parameters of Ni^{2+} and Pd^{2+} complexes (vide infra) were also included. The very good agreement between the found geometric parameters and those estimated by using DFT calculations is clear in Figure 8, which shows both the found molecular structure and the calculated model.

As these crystals belong to the centrosymmetric $P2_1/n$ space group, the compound crystallizes as a racemate. Apart from an intramolecular H bond (Table 1), corresponding to the major component of a bifurcated H bond,[25] another factor that clearly influences the molecular conformation is the $\pi-\pi$ stacking. This is evidenced by the interaction that exists between the two

dx.doi.org/10.1021/ic2017038 | Inorg. Chem. 2012, 51, 1278−1293

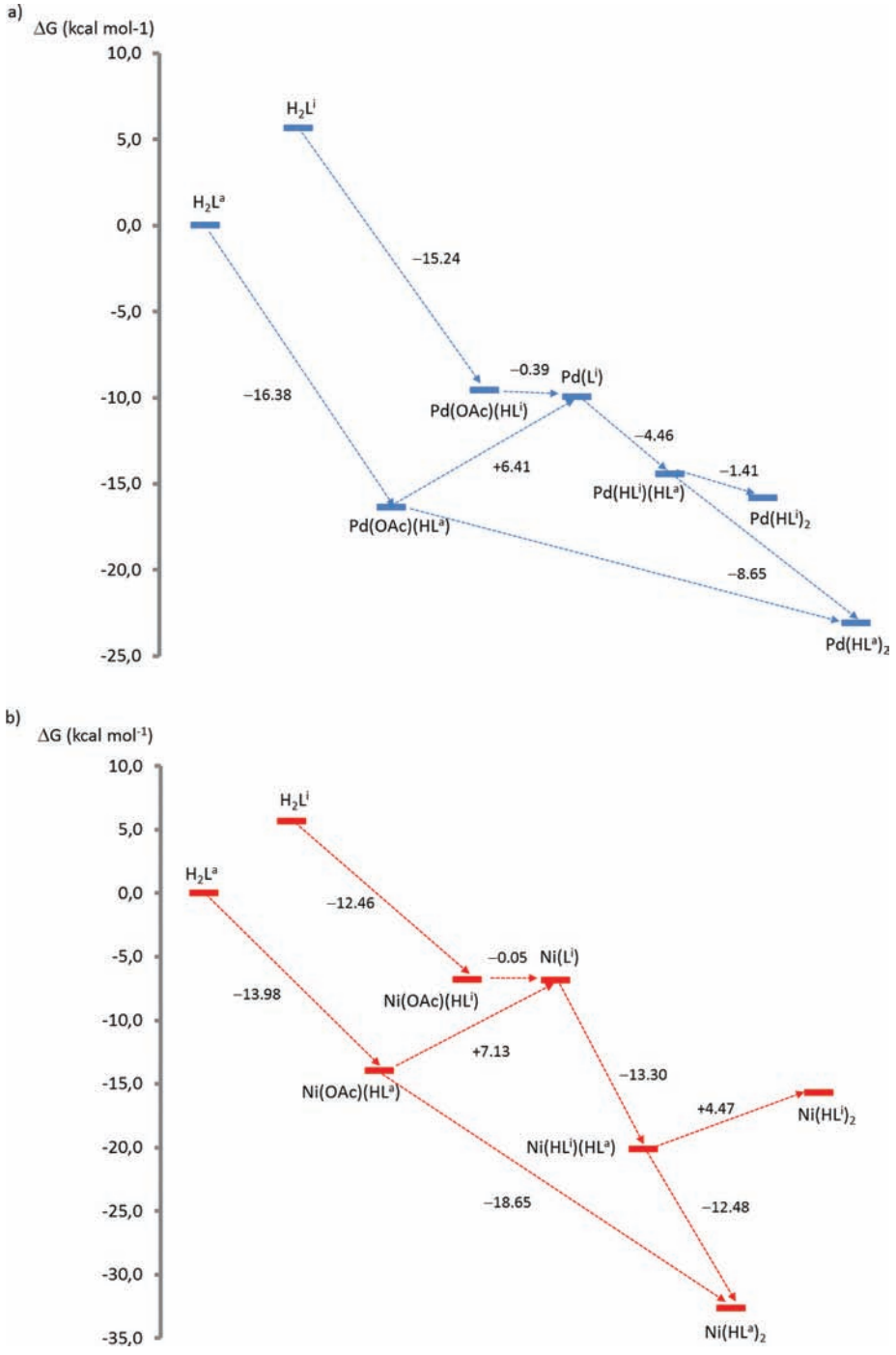

Figure 6. Complete Gibbs free energy profiles for the reactions between the closed-chain tetrahydroquinazoline H_2L^a and open-chain imine H_2L^i with (a) $Pd(OAc)_2{\cdot}4H_2O$ and (b) $Ni(OAc)_2{\cdot}4H_2O$.

aromatic rings of the tosyl and diamine residues, with a distance of ca. 3.7 Å between their respective centroids.

Crystal Structures of $Ni(HL^a)_2{\cdot}2HOAc$ and $Ni(HL^a)_2{\cdot}4MeOH$. The asymmetric unit of $Ni(HL^a)_2{\cdot}2HOAc$ only includes half a molecule of the neutral complex, and this is accompanied by an acetic acid molecule, which is doubly interacting through N−H···O and O−H···O contacts with the complex molecule (Table 2). The complete molecule (Figure 9) is generated by means of the symmetry operation $-x + {}^1/_2$, y, $-z + 1$, related with a C_2 rotation axis parallel to b, which goes through the nickel(II) ion.

The $Ni(HL^a)_2{\cdot}4MeOH$ crystal is formed by crystallographically independent molecules of the neutral nickel(II) complex along with some solvated methanol molecules with partial occupation sites, which interact through H bonding (Table 2). The *O* atoms of one of the tosyl groups are disordered on two sites with an occupation ratio of 0.93:0.07. An ellipsoid diagram of the neutral complex is shown in Figure 10, for which the labeling scheme is equivalent to that of the free ligand, but either preceded by 1 or 2, or using "a" or "b", for each of the coordinated ligands.

The crystal structures of both $Ni(HL^a)_2{\cdot}2HOAc$ and $Ni(HL^a)_2{\cdot}4MeOH$ are very similar as they consist of a

dx.doi.org/10.1021/ic2017038 | *Inorg. Chem.* 2012, 51, 1278−1293

Scheme 4. General Proposed Mechanism for the Conversion of M(OAc)(HL^a) to M(L^i) and M(HL^a)$_2$[a]

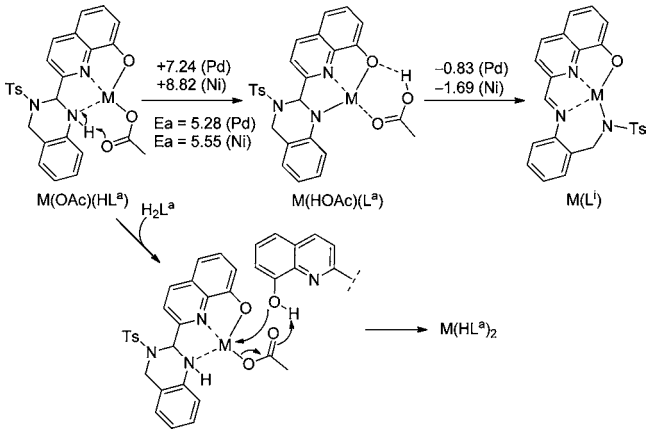

[a]Gibbs free energy difference (kcal mol^{-1}) of the studied steps is indicated.

nickel(II) ion coordinated to two monoanionic units of tetrahydroquinazoline ligand with a practically planar extended π-conjugated system. (HL^a)$^-$ units act as tridentate donors through the *N*,*O* set of the quinoline, where the hydroxyl group of which is deprotonated, in conjunction with the protonated amine *N* atom of the tetrahydroquinazoline moiety.

The Ni^{2+} coordination polyhedrons can be described as distorted octahedrons, with the axial positions occupied by the $N_{quinoline}$ atoms. Since the Ni−$N_{quinoline}$ bonds are the shortest for this coordination environment (Table 2), these polyhedrons are more compressed than elongated, and each *N*,*N*,*O*-donor set occupies a pseudomeridian. This spatial disposition leads to a typical double-blade propeller arrangement around the nickel ion, which involves chirality and will be further discussed in the corresponding section.

Both Ni(HL^a)$_2$·2HOAc and Ni(HL^a)$_2$·4MeOH show π−π stacking interactions between tetrahydroquinazoline and tosyl rings, as occurred in the free ligand, while interactions between neighboring tetrahydroquinazoline rings are patently different and related to C−H···π contacts. Thus, for Ni(HL^a)$_2$·2HOAc there are two mutual interactions through one of the methylene H atoms of each ligand unit, whereas in Ni(HL^a)$_2$·4MeOH there is only one CH−π interaction between them, by means of a methine *H* atom.

To see if the theoretical methods reproduce the experimental geometries of the Ni(II) complexes their structures were optimized using DFT calculations with M06 functional.[18,19] The experimental and calculated structures are compared in Supporting Information through their geometrical data. The agreement is very good, suggesting that the level of calculation is relevant to study these complexes.

Crystal Structure of Pd(L^i)·CH$_2$Cl$_2$. The asymmetric unit of this crystal structure contains one molecule of the neutral

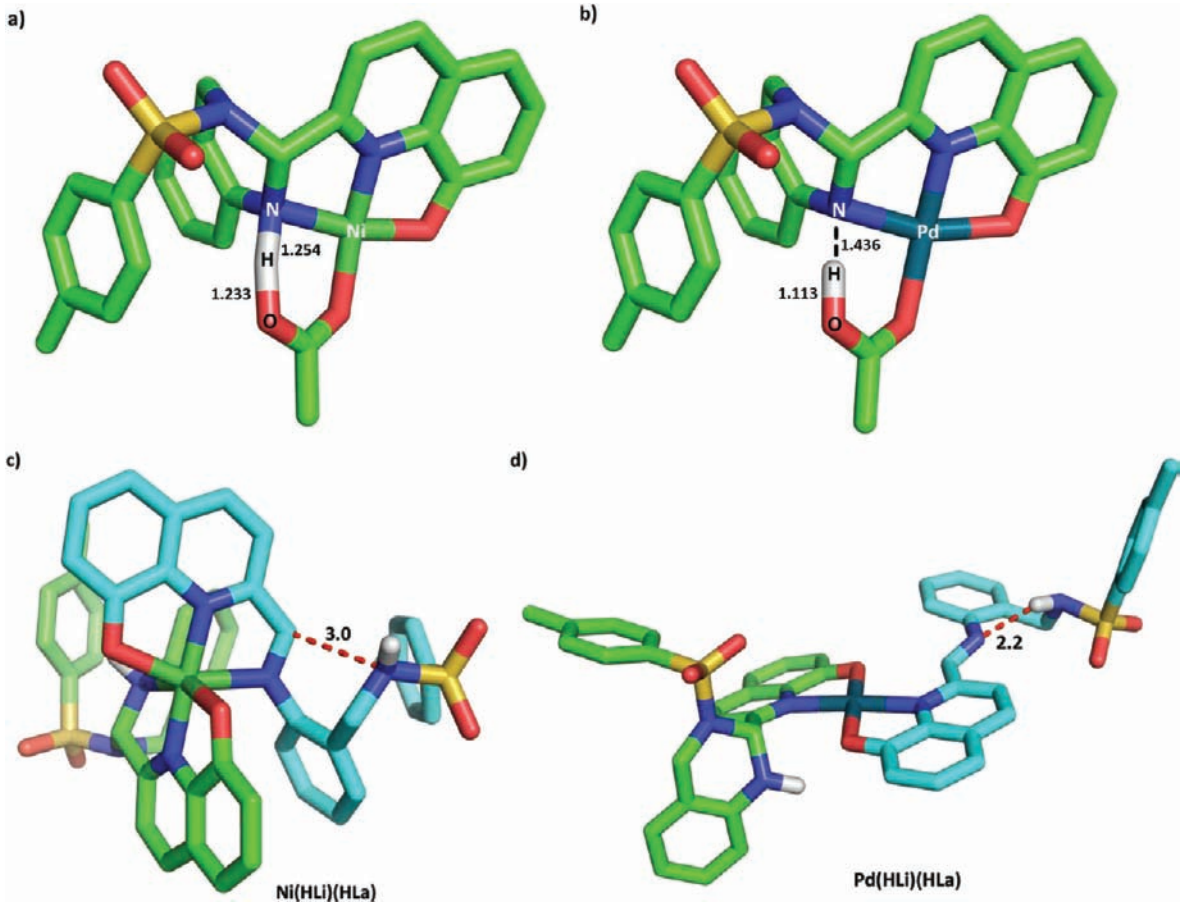

Figure 7. Transition states for the intramolecular proton abstraction step involving the conversion of M(OAc)(HL^a) into M(HOAc)(L^a) (**a** for M = Ni and **b** for M = Pd) and structures of the most stable conformers of intermediate complexes Ni(HL^i)(HL^a) and Pd(HL^i)(HL^a) (**c** and **d**). Relevant distances are indicated.

dx.doi.org/10.1021/ic2017038 | *Inorg. Chem.* 2012, 51, 1278−1293

Table 1. Main Bond Distances [Å] and Angles [deg] for H_2L^a Collected in the First Column with Equivalent Parameters for $Ni(HL^a)_2\cdot 2HOAc$, $Ni(HL^a)_2\cdot 4MeOH$, and $Pd(L^i)\cdot CH_2Cl_2$ Included for Ease of Comparison with Configurations of Stereogenic Centers of the Ligand Molecules Also Indicated

	H_2L^a	$Ni(HL^a)_2\cdot 2HOAc$	$Ni(HL^a)_2\cdot 4MeOH^b$		
	R^a	$C(R)N(S)^a$	$C(R)N(S)^a$	$C(S)N(R)^a$	$Pd(L^i)\cdot CH_2Cl_2$
Distance[c]					
N1−C2	1.316(3)	1.328(6)	1.316(3)	1.316(3)	1.336(8)
N1−C8A	1.374(3)	1.363(5)	1.358(3)	1.362(3)	1.343(8)
C8−O1	1.355(3)	1.337(5)	1.311(3)	1.315(3)	1.339(8)
C9−N2	1.443(3)	1.499(5)	1.494(3)	1.486(3)	1.305(8)
N2−C9A	1.382(4)	1.435(6)	1.443(3)	1.424(3)	1.428(9)
C9−N3	1.470(3)	1.451(5)	1.457(3)	1.458(3)	
C13A−C14	1.512(4)	1.514(6)	1.501(4)	1.507(4)	1.507(9)
C14−N3	1.476(3)	1.476(6)	1.474(3)	1.470(3)	1.483(8)
N3−S1	1.645(2)	1.654(4)	1.650(2)	1.645(2)	1.600(3)
S1−C15	1.765(3)	1.746(5)	1.760(3)	1.759(3)	1.770(7)
Angle[d]					
C2−N1−C8A	117.5(2)	119.4(4)	121.0(2)	120.6(2)	124.7(6)
N1−C2−C3	123.5(2)	121.8(4)	121.1(2)	121.4(2)	118.0(6)
C9−N2−C9A	118.6(2)	117.4(4)	117.08(19)	117.9(2)	121.3(6)
C9−N3−C14	112.4(2)	112.0(4)	111.8(2)	113.50(19)	
C9−N3−S1	118.62(17)	118.2(3)	118.67(18)	121.13(17)	
C14−N3−S1	116.54(17)	119.3(3)	119.43(17)	118.96(17)	114.1(4)
C13A−C14−N3	111.0(2)	109.4(4)	110.1(2)	109.4(2)	113.9(6)
N3−S1−C15	107.72(12)	108.6(2)	107.98(12)	108.58(11)	108.8(3)
Torsion[d]					
O1−C8−C8A−N1	−1.9(4)	0.2(6)	2.6(3)	0.6(3)	−0.1(8)
N1−C2−C9−N2	−20.8(3)	21.4(6)	16.1(3)	−5.4(3)	1.9(9)
N2−C9A−C13A−C14	2.7(4)	9.7(6)	7.8(4)	−9.1(3)	0.9(10)
N1−C2−C9−N3	−142.6(2)	147.9(4)	141.7(2)	−131.6(2)	
C2−C9−N2−C9A	−77.0(3)	121.0(4)	108.0(2)	−119.7(2)	178.5(6)
C9−N2−C9A−C13A	−15.6(4)	−25.8(6)	−15.7(3)	23.9(3)	−158.9(6)
C14−N3−S1−C15	55.1(2)	−72.1(4)	−64.9(2)	55.1(2)	−69.5(5)
S1−N3−C9−N2	79.9(2)	−99.2(4)	−93.8(2)	106.7(2)	
C9A−N2−C9−N3	43.8(3)	−2.6(6)	−14.3(3)	3.5(3)	
N2−C9−N3−S1	79.9(2)	−99.2(4)	−93.8(2)	106.7(2)	
N2−C9−N3−C14	−60.9(3)	45.4(5)	51.4(3)	−44.9(3)	
C13A−C14−N3−S1	−93.3(2)	84.3(4)	86.9(2)	−94.1(2)	−147.7(5)
C9A−C13A−C14−N3	−19.2(3)	32.4(6)	28.7(3)	−30.9(3)	−46.7(3)
C14−N3−S1−C15	55.1(2)	−72.1(4)	−64.9(2)	55.1(2)	−69.5(5)
D−H···A	d(D−H)[c]	d(D···A)[c]	<(DHA)[d]	D−H···A	
H Bond Scheme for H_2L^e					
O1−H1···N1	0.80(5)	2.714(3)	123(4)	O1−H1···N1	
O1−H1···O2$^{\#1}$	0.80(5)	2.917(3)	131(4)	O1−H1···O2$^{\#1}$	
N2−H2A···N3$^{\#2}$	0.82(3)	3.013(3)	119(3)	N2−H2A···N3$^{\#2}$	
N2−H2A···O2$^{\#1}$	0.82(3)	3.465(3)	151(3)	N2−H2A···O2$^{\#1}$	

[a]Chirality of the stereogenic centers for the enantiomers found in the respective asymmetric units. [b]Despite the different labeling schemes, the parameters compared are totally equivalent. [c]In Å. [d]In deg. [e]Symmetry transformations used to generate equivalent atoms: $^{\#1}$ $x, y, z-1$, $^{\#2}$ $x, -y+{}^1/_2, z-{}^1/_2$.

palladium(II) complex along with a solvated dichloromethane molecule. An ORTEP diagram of $Pd(L^i)$ is shown in Figure 11, and the main bond distances and angles for the coordination environment are collected in Table 2.

Since these crystals were obtained from a reaction in which H_2L^a was the starting material, the molecular structure of $Pd(L^i)\cdot CH_2Cl_2$ not only demonstrates tetrahydroquinazoline ring-opening due to coordination to palladium(II), but also the 180° turn around the C2−C9 bond. As a result, the two bidentate *N,N* and *N,O* domains are *endo* positioned instead of *exo*, as occurred for H_2L^i. Hence, the metal ion is tetracoordinated to the *O,N,N,N* donor set that provides the open imine H_2L^i after bideprotonation. This disposition enables a practically planar and pseudosquare environment, where the metal ion protrudes very little (0.017 Å) from the calculated least-squares plane formed by the four donor atoms.

Chirality. In solid state, H_2L^a has one chiral atom (C9) and two prochiral ones (N2 and N3) with same configuration (*R,R,R*) or (*S,S,S*) as shown in Figure 12, top, but in solution, the energetic barriers should be too low to avoid this structure flipping inside out. It must be noted that as a result of the metal coordination the configurations of C9 reverse due to changes in the Cahn−Ingold−Prelog conventions, as Figure 12 shows.

dx.doi.org/10.1021/ic2017038 | *Inorg. Chem.* 2012, 51, 1278−1293

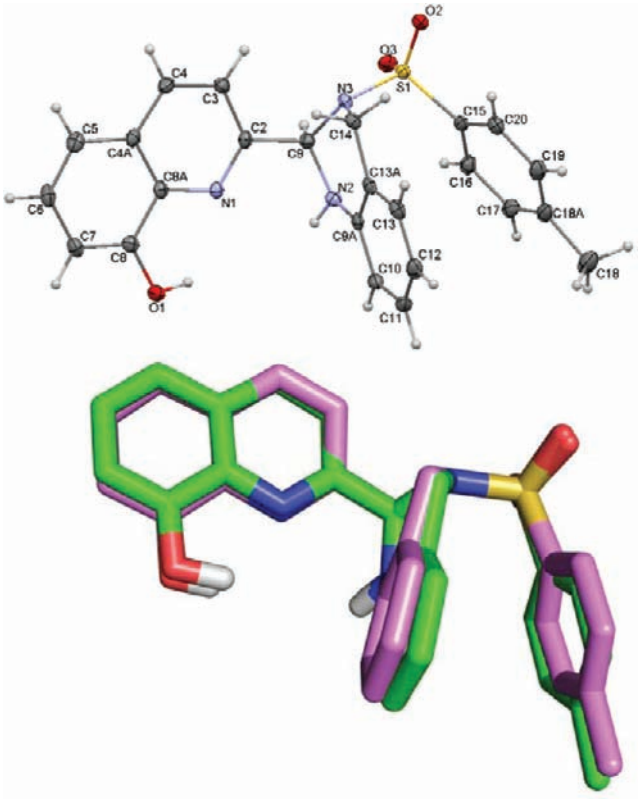

Figure 8. Molecular structure of 2-(1,2,3,4-tetrahydro-3-tosylquinazolin-2-yl)quinolin-8-ol. The figure (top) shows the *R* enantiomer of (*rac*)-H_2L^a with ellipsoids at the 50% probability level. Comparison (bottom) of the calculated structure (DFT/M06 level in methanol) of H_2L^a (green) and the experimental X-ray structure of H_2L^a (violet).

Both $Ni(HL^a)_2{\cdot}2HOAc$ and $Ni(HL^a)_2{\cdot}4MeOH$ are chiral not only because they combine the *R* and *S* enantiomers of the aminal ligand, but also because they are helical. Thus, (Δ,Λ)-racemates can be considered for these complexes in the unit cell, as the crystal structures correspond to nonchiral space groups. For the nomenclature of these helicates, the helicity (Δ,Λ) will be first indicated and second, the configurations (*R*,*S*) of the two ligand units arranged in accordance with the numbering scheme (100 and 200 series) for chiral atoms C9 and N2, respectively. Figure 12, middle, shows a representation of $Ni(HL^a)_2{\cdot}4MeOH$ that combines the *R* and *S* enantiomers of the aminal ligand. In this complex, each helical enantiomer (Δ,Λ) comprises both *R* and *S* enantiomers of $(HL^a)^-$, so its racemate can be described as [Δ,Λ-C(*R*,*S*)N(*S*,*R*)]-Ni-$(HL^a)_2{\cdot}4MeOH$. In contrast, each Δ and Λ enantiomer found for $Ni(HL^a)_2{\cdot}2HOAc$ involves two enantiomers of $(HL^a)^-$ of identical chirality. Thus, two *R* enantiomers of $(HL^a)^-$ are coordinated in the Λ isomer, while two *S* enantiomers of $(HL^a)^-$ form the Δ isomer, as shown at the bottom of Figure 12. Consequently, its racemate could be described as [Δ-C(*R*,*R*)N(*S*,*S*),Λ-C(*S*,*S*)N(*R*,*R*)]-Ni-$(HL^a)_2{\cdot}2HOAc$.

To understand the origin of the formation of two isomers among the three possible ones, [Δ,Λ-C(*R*,*S*)N(*S*,*R*)]-$Ni(HL^a)_2$ (Figure 13, bottom), [Δ-C(*R*,*R*)N(*S*,*S*),Λ-C(*S*,*S*)N(*R*,*R*)]-Ni-$(HL^a)_2$ (Figure 13, top), and hypothetical [Δ-C(*S*,*S*)N(*R*,*R*),Λ-C(*R*,*R*)N(*S*,*S*)]-$Ni(HL^a)_2$, their relative stabilities were investigated. Molecular modeling studies at the DFT level by means of the hybrid M06 functional[18,19] (vide supra) predicted that the isomers [Δ-C(*S*,*S*)N(*R*,*R*)]-$Ni(HL^a)_2$ and [Λ-C(*S*,*R*)N-(*R*,*S*)]-$Ni(HL^a)_2$ are virtually isoenergetic (Figure 5). The not experimentally found isomer [Δ-C(*R*,*R*)N(*S*,*S*)]-$Ni(HL^a)_2$ is 4.9 kcal mol^{-1} less stable than those stereoisomers found for crystallized $Ni(HL^a)_2{\cdot}2HOAc$ and $Ni(HL^a)_2{\cdot}4MeOH$.

Finally, it is worthy of mention that the helical chirality of $Pd(L^i){\cdot}CH_2Cl_2$ is merely conformational, as it could disappear in solution since it is only based on the conformation of the methylene group and the orientation of the tosyl group. This situation is illustrated in Figure 14, in which the Δ and the Λ isomers are represented.

CONCLUSIONS AND FINAL REMARKS

The final product of the condensation reaction of 8-hydroxyquinoline-2-carboxaldehyde with *N*-(2-aminobenzyl)-4-methylbenzenesulfonamide strongly depends on the reaction time. Indeed, reaction times of about 1 h gave the open-chain imine (*E*)-*N*-{2-[(8-hydroxy-quinolin-2-yl)-methyleneamino]-benzyl}-4-methyl-benzenesulfonamide (H_2L^i) as the main product. However, when the reaction time exceeded 4.5 h, the chiral cyclic aminal *rac*-2-(3-tosyl-1,2,3,4-tetrahydroquinazolin-2-yl)quinolin-8-ol (H_2L^a) was exclusively obtained. The tetrahydroquinazoline compound H_2L^a is the most stable form of the two tautomers, and the intramolecular ring-closing reaction of H_2L^i to give H_2L^a is energetically favored, as evidenced by DFT calculations.

The aforementioned ring−chain tautomerism has been exploited to induce reversible changes in the aminal−imine equilibrium, as desired, by coordination of a suitable metal ion. The cyclic tautomeric form of the equilibrium studied is retained upon fast complexation of tetrahydroquinazoline H_2L^a to nickel(II) to yield complexes of the type $Ni(HL^a)_2$, where the aminal ligand behaves as a tridentate *N*,*N*,*O*-donor. The same complex was obtained on using imine H_2L^i as ligand, what means that Ni^{2+} causes imine H_2L^i to undergo a ring-closing cyclization process on coordination. In contrast, tetrahydroquinazoline H_2L^a undergoes a ring-opening reaction on complex formation with Pd^{2+} to yield $Pd(HL^i)_2{\cdot}MeOH$, in which the linear imine only acts as a bidentate ligand through the *N*,*O* donor set of the 8-hydroxyquinoline residue. The selective ring-opening is related to the rapidly formed $Pd(L^i){\cdot}CH_2Cl_2$, in which the linear ligand acts as a tetracoordinate *N*,*N*,*N*,*O*-donor. This subsequently yields $Pd(HL^i)_2{\cdot}MeOH$, in which the ligand has a helical arrangement.

The aminal tautomer H_2L^a is predisposed to a planar *N*,*N*,*O* tricoordinate behavior, without apparent changes after complexation. In pseudo-octahedral coordination environments, as preferred by Ni^{2+} ions, each ligand occupies a pseudomeridian, which gives rise to a typical double-blade propeller disposition and therefore to Λ and Δ enantiomers. These enantiomers can combine two ligand units with identical or different chirality. Thus, we determined the crystal structures of two racemates: [Δ-C(*R*,*R*)N(*S*,*S*),Λ-C(*S*,*S*)N(*R*,*R*)]-Ni-$(HL^a)_2{\cdot}2HOAc$ and [Δ,Λ-C(*R*,*S*)N(*S*,*R*)]-$Ni(HL^a)_2{\cdot}4MeOH$. DFT studies carried out for the possible diastereoisomers indicate that [Λ-C(*S*,*S*)N(*R*,*R*)]-$Ni(HL^a)_2$ and [Λ-C(*R*,*S*)N-(*S*,*R*)]-$Ni(HL^a)_2$ are 4.3 and 4.9 kcal mol^{-1}, respectively, more stable than [Λ-C(*R*,*R*)N(*S*,*S*)]-$Ni(HL^a)_2$, and which was not experimentally found. Combined structural and theoretical calculations show that models obtained from DFT calculations reproduce the geometry of the crystallized compounds.

dx.doi.org/10.1021/ic2017038 | *Inorg. Chem.* 2012, 51, 1278−1293

Table 2. Main Bond Distances [Å] and Angles [deg] for the Coordination Environments of $Ni(HL^a)_2 \cdot 2HOAc$, $Ni(HL^a)_2 \cdot 4MeOH$, and $Pd(L^i) \cdot CH_2Cl_2$

$Ni(HL^a)_2 \cdot 2HOAc$		$Ni(HL^a)_2 \cdot 4MeOH$		$Pd(L^i) \cdot CH_2Cl_2$	
distance[a]		distance[a]		distance[a]	
Ni1–N1	1.973(3)	Ni1–N101	1.9672(19)	Pd1–N1	1.929(5)
Ni1–N1$^{\#1,c}$	1.973(3)	Ni1–N201	1.9581(19)		
Ni1–O1	2.054(3)	Ni1–O101	2.0388(17)	Pd1–O1	2.082(4)
Ni1–O1$^{\#1}$	2.054(3)	Ni1–O201	2.0484(16)		
Ni1–N2	2.394(4)	Ni1–N102	2.382(2)	Pd1–N2	2.027(5)
Ni1–N2$^{\#1}$	2.394(4)	Ni1–N202	2.292(2)	Pd1–N3	2.007(5)
angle[b]		angle[b]		angle[b]	
N1–Ni1–N1$^{\#1}$	167.2(2)	N101–Ni1–N201	179.00(9)	N1–Pd1–N3	172.9(2)
N1–Ni1–O1$^{\#1}$	107.92(13)	N101–Ni1–O201	97.94(7)	N1–Pd1–N2	80.0(2)
N1$^{\#1}$–Ni1–O1$^{\#1}$	80.92(14)	N201–Ni1–O201	81.78(7)	N3–Pd1–N2	93.0(2)
N1–Ni1–O1	80.93(14)	N101–Ni1–O101	82.86(8)	N1–Pd1–O1	80.8(2)
N1$^{\#1}$–Ni1–O1	107.92(13)	N201–Ni1–O101	98.11(7)	N3–Pd1–O1	106.2(2)
O1$^{\#1}$–Ni1–O1	95.56(18)	O101–Ni1–O201	93.95(7)	N2–Pd1–O1	160.79(19
N1–Ni1–N2$^{\#1}$	96.80(14)	N101–Ni1–N202	103.07(8)	N1–Ni1–N2$^{\#1}$	
N1$^{\#1}$–Ni1–N2$^{\#1}$	75.37(14)	N201–Ni1–N202	77.19(8)	N1$^{\#1}$–Ni1–N2$^{\#1}$	
O1$^{\#1}$–Ni1–N2$^{\#1}$	154.99(12)	O201–Ni1–N202	158.95(7)	O1$^{\#1}$–Ni1–N2$^{\#1}$	
O1–Ni1–N2$^{\#1}$	84.38(14)	O101–Ni1–N202	89.89(8)	O1–Ni1–N2$^{\#1}$	
N1–Ni1–N2	75.37(14)	N101–Ni1–N102	75.49(8)	N1–Ni1–N2	
N1$^{\#1}$–Ni1–N2	96.80(14)	N201–Ni1–N102	103.54(8)	N1$^{\#1}$–Ni1–N2	
O1$^{\#1}$–Ni1–N2	84.37(14)	O201–Ni1–N102	89.26(7)	O1$^{\#1}$–Ni1–N2	
O1–Ni1–N2	154.99(12)	O101–Ni1–N102	158.35(7)	O1–Ni1–N2	
N2$^{\#1}$–Ni1–N2	106.1(2)	N202–Ni1–N102	94.77(8)	N2$^{\#1}$–Ni1–N2	
D–H···A	d(D–H)[a]	d(D···A)[a]	<(DHA)[b]		
H-Bond Scheme for $Ni(HL^a)_2 \cdot 2HOAc$					
N2–H2A···O31$^{\#1}$	0.94(5)	3.009(5)	140(4)		
N2–H2A···O31$^{\#1}$	0.94(5)	3.009(5)	140(4)		
N2–H2A···O1$^{\#1}$	0.94(5)	2.997(5)	110(4)		
O30–H30···O1	1.11	2.519(4)	176		
H-Bond Scheme for $Ni(HL^a)_2 \cdot 4MeOH$					
N202–H22···O1S	0.80(3)	2.888(3)	164		
O1S–H1S···O4S	0.99	2.731(4)	148		
O1S–H1S···O4S′	0.99	2.336(19)	134		
O2S–H2S···O3S	0.84	2.689(3)	170		
O3S–H3S···O201	0.84	2.613(2)	168		
O4S–H4S···O2S$^{\#2}$	0.84	2.710(3)	170		

[a]In Å. [b]In deg. [c]Symmetry transformations used to generate equivalent atoms: $^{\#1}$ $-x+2, y, -z+{}^1/_2$. $^{\#2}$ $x, y+1, z$.

Experimental data and theoretical studies suggest that the formation of these complexes involves initially the metal promoted ring-opening reaction of the tetrahydroquinazoline H_2L^a to give $M(L^i)$ than then evolves to $Pd(HL^i)_2$ or $Ni(HL^a)_2$ via the intermediate complexes $M(HL^i)(HL^a)$. The coordination of the imine present in $Ni(HL^i)(HL^a)$ allows a subsequent intramolecular ring-closing reaction of the open-chain ligand to afford $Ni(HL^a)_2$. The opposite conversion, i.e., the intramolecular ring-opening reaction of the aminal in $Ni(HL^i)(HL^a)$ to give $Ni(HL^i)_2$, is energetically unfavorable. In contrast, the square planar coordination of Pd^{2+} in $Pd(HL^i)(HL^a)$ does not promote a similar metal assisted ring-closing reaction of open-chain ligand, but an intramolecular ring-opening reaction to give $Pd(HL^i)_2$. While for Pd^{2+}, the reaction always goes via $Pd(L^i)$, for Ni^{2+}, when a 1:2 molar ratio is used, the experimentally obtained complex $Ni(HL^a)_2$ is probably formed by direct displacement of the acetate ligand in $Ni(OAc)(HL^a)$ by another molecule of H_2L^a.

The studies described here allow us to conclude that Ni^{2+} and Pd^{2+} coordination can be used to induce closing and opening reactions of a tetrahydroquinazoline ring. These processes are directed by the coordinative preferences of the metal in its complexes: While Ni^{2+} in octahedral environment stabilizes the tridentate closed-chain tautomer, the preference of Pd^{2+} for a square planar environment leads to a tetra- or bidentate behavior of the open-chain tautomer.

EXPERIMENTAL SECTION

General Procedures. All starting materials and reagents were commercially available without further purification. Elemental analyses were performed on a Carlo Erba EA 1108 analyzer. Positive electrospray ionization mass spectra were recorded on an LC/MSD Hewlett-Packard 1100 spectrometer, using methanol as solvent (2% formic acid). The mass spectrometry samples were previously dissolved in the minimum amount of dimethylsulfoxide. NMR spectra were recorded on Bruker spectrometers using DMSO-d_6 as solvent. NMR assignments were made by a combination of DEPT-135, HMQC, HMBC, COSY, NOESY, and NOE experiments. Infrared spectra were recorded as KBr pellets on a Bio-Rad FTS 135 spectrophotometer in the range 4000–600 cm^{-1}. UV–vis spectra were performed on 10^{-4}–10^{-5} M methanol solutions with a CECIL CE 2021 spectrophotometer.

dx.doi.org/10.1021/ic2017038 | Inorg. Chem. 2012, 51, 1278–1293

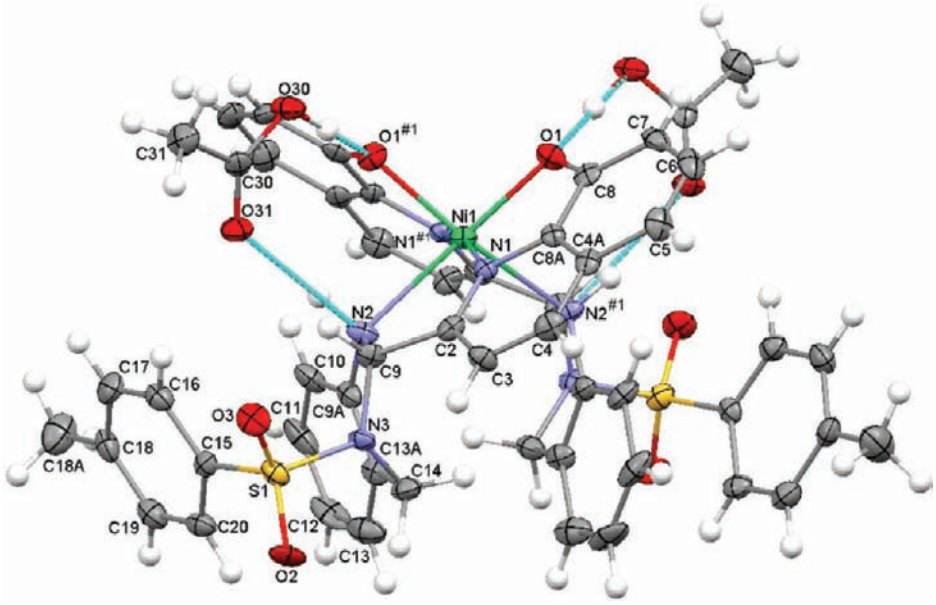

Figure 9. Ellipsoid representation at the 50% probability level of the molecular structure of $Ni(HL^a)_2 \cdot 2AcOH$. The double H bonding interaction between $Ni(HL^a)_2$ and two acetic acid molecules trapped as solvates is also indicated. The labeling scheme is similar to that used for the free ligand H_2L^a. The figure shows the Δ-C(*R*,*R*)N(*S*,*S*) enantiomer.

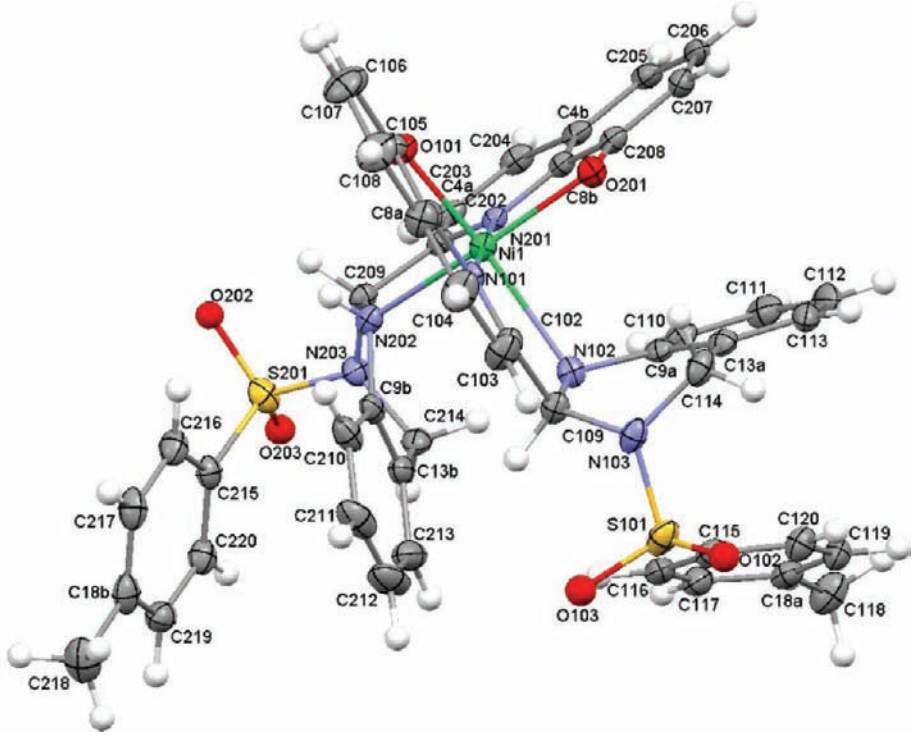

Figure 10. ORTEP representation of the molecular structure of the $Ni(HL^a)_2$ complex found in $Ni(HL^a)_2 \cdot 4MeOH$. Solvates have been omitted for clarity. Ellipsoids are represented at the 50% probability level. The figure shows the Λ-C(*R*,*S*)N(*S*,*R*) enantiomer.

Crystal Structure Analysis Data. Diffraction data for H_2L^a, $Ni(HL^a)_2 \cdot 2HOAc$, $Ni(HL^a)_2 \cdot 4MeOH$, and $Pd(L^i) \cdot CH_2Cl_2$ were collected at 100(2) K, using graphite-monochromated Mo Kα radiation (λ = 0.710 73 Å) from a fine focus sealed tube. Some significant crystal parameters and refinement data are summarized in Table 3. Data were processed and corrected for Lorentz and polarization effects. Multiscan absorption corrections were performed using the SADABS routine.[26] Structures were solved by standard direct methods[27] and then refined by full matrix least-squares on F^2.[28] All non-hydrogen atoms were anisotropically refined, except those that were disordered and had lower occupation sites for $Ni(HL^a)_2 \cdot 4MeOH$. Hydrogen atoms were mostly included in the structure factor calculation in geometrically idealized positions, with thermal parameters depending on the parent atom, by using a riding model. In most cases, the H atoms that were potentially involved in the H bonding schemes were located in Fourier maps and isotropically treated.

However, there is a significant exception to the latter comment related to $Ni(HL^a)_2 \cdot 2HOAc$. In this case, ΔF maps showed electron densities at chemically reasonable positions near to one of the *O* atoms

dx.doi.org/10.1021/ic2017038 | *Inorg. Chem.* 2012, 51, 1278–1293

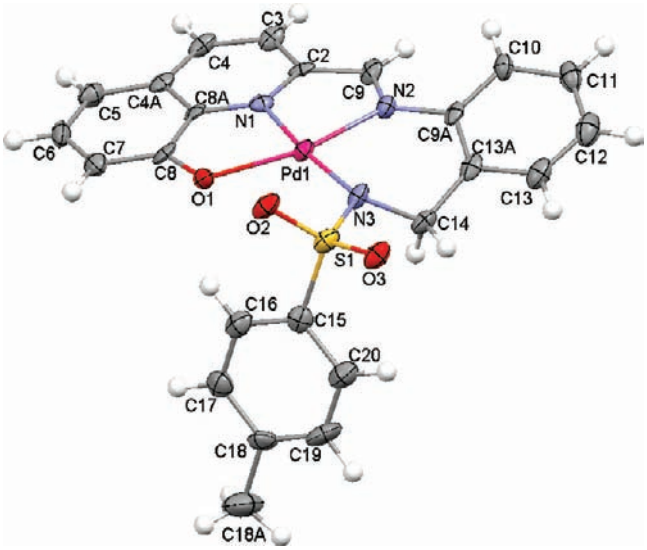

Figure 11. Ellipsoid representation at the 50% probability level of the molecular structure solved for Pd(L^i). H atoms and solvates have been omitted for clarity.

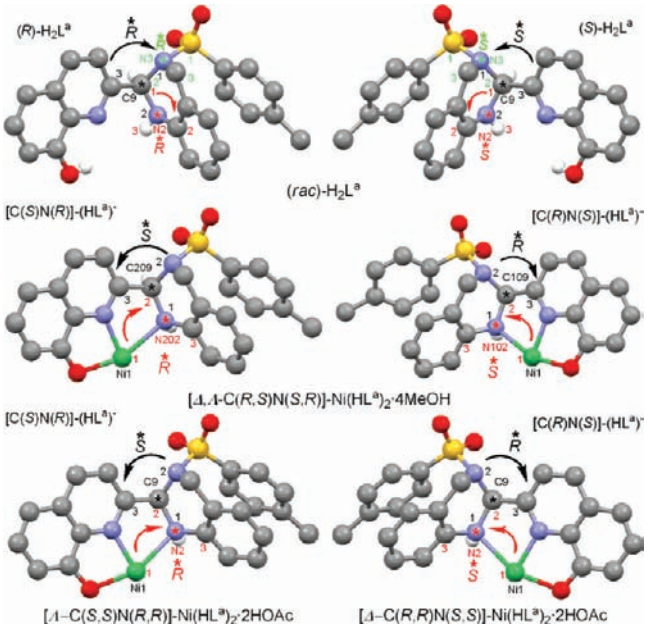

Figure 12. Ball and stick representations of (top) the two enantiomers of H_2L^a as free ligand, (middle) both monodeprotonated and coordinated ligand units in Ni(HL^a)$_2$·4MeOH and in (bottom) Ni(HL^a)$_2$·2HOAc.

of the acetate fragment. When this was freely refined, this H atom appeared nearer to the O1 atom of the coordinated ligand. Therefore, some related bond distances were thoroughly investigated by means of a search in the Cambridge Structural Database.[29] Thus, in nickel(II) complexes, distances for coordinated Ph−O and Ph−OH average 1.310 and 1.358 Å, respectively. In this case study, d(C8−O1) = 1.337(5) Å shows an intermediate value between relatively common values reported for Ni−O−Ph interactions [1.237−1.366 Å] and that is practically at the lowest extreme of the range reported for Ni−OH−Ph bonds [1.337−1.378 Å].[30] In addition, the clear dissimilarity of the two C−O bonds of the acetate fragment, 1.320(5) and 1.212(5) Å, seems more indicative of a neutral rather than an anionic nature. Hence, the coordinates of this hydrogen atom were freely refined, but its isotropic thermal parameter was set at 1.2 times the isotropic

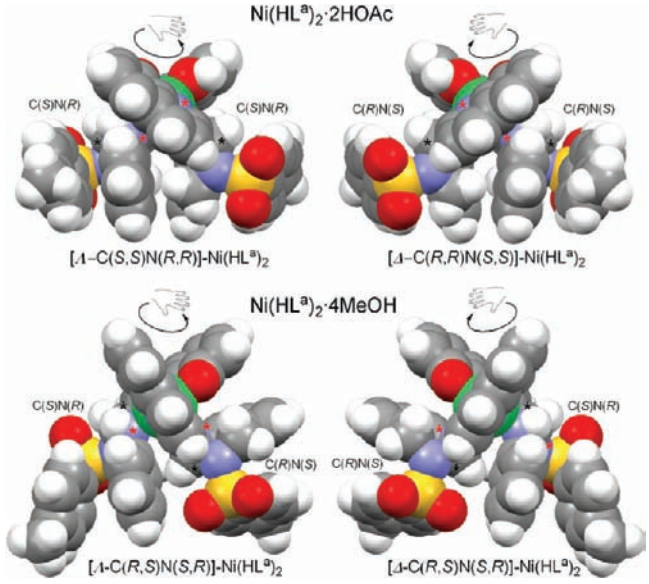

Figure 13. Spacefill representations of the helical Λ (left) and Δ (right) enantiomers of the two Ni(HL^a)$_2$ complexes studied here. Chiral centers are marked with * (red for *N*, black for *C*) for ease of understanding.

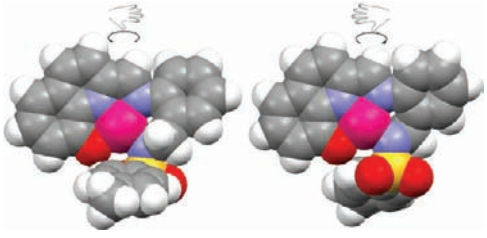

Figure 14. Spacefill representation of the Λ (left) and Δ (right) helical enantiomers found for Pd(L^i) in the crystal structure of Pd(L^i)·CH_2Cl_2.

equivalent of the parent O atom corresponding to the acetic acid. The notable length of this bond, with the H atom at 1.11 Å from the O atom (Table 2), and the short O···O distance indicate the strength of this interaction and could also indicate an intermediate situation between the coordinated ligand and the acetic acid molecules. All the above facts could point to a mixture of complexes with cationic and neutral natures. However, as possible disorder could not be adequately modeled, and according to the distance values mentioned, a formula of the type Ni(HL^a)$_2$·2HOAc was assumed instead of [Ni(H_2L^a)$_2$](OAc)$_2$.

CCDC 814044−814047 contain the supplementary crystallographic data for this paper. These data can be obtained free of charge from The Cambridge Crystallographic Data Centre via www.ccdc.cam.ac.uk/data_request/cif.

Theoretical Studies. All calculations were performed by using the Gaussian 09W[17] program package at density functional theory (DFT) level by means of the hybrid M06[18,19] functional. The standard 6-31G(d) basis set was used for C, H, O, S, and N, and the LANL2DZ relativistic pseudopotential was used for Pd and Ni. The starting point of these calculations was the crystallographic structures described in this Article, the tetrahydroquinozinoline H_2L^a and its Pd^{II} and Ni^{II} metal complexes. First, the crystallographic structures obtained were minimized at a DFT level. The resulting energy value was taken as a reference for all subsequent calculations. On the optimized geometries a DFT minimization in methanol solution by means of the polarizable continuum solvation model[20] was performed. Harmonic frequencies were calculated at the same level of theory to characterize the stationary points and to determine the zero-point energies (ZPEs). All

dx.doi.org/10.1021/ic2017038 | Inorg. Chem. 2012, 51, 1278−1293

Table 3. Diffraction Data for H_2L^a, $Ni(HL^a)_2{\cdot}2HOAc$, $Ni(HL^a)_2{\cdot}4MeOH$, and $Pd(L^i){\cdot}CH_2Cl_2$

	H_2L^a	$Ni(HL^a)_2{\cdot}2HOAc$	$Ni(HL^a)_2{\cdot}4MeOH$	$Pd(L^i){\cdot}CH_2Cl_2$
formula	$C_{24}H_{21}N_3O_3S$	$C_{52}H_{48}N_6NiO_{10}S_2$	$C_{52}H_{56}N_6NiO_{10}S_2$	$C_{25}H_{21}Cl_2N_3O_3PdS_5$
M_r	431.50	1039.79	1047.86	620.81
cryst syst	monoclinic	monoclinic	triclinic	orthorhombic
space group	$P2_1/n$	$C2/c$	$P\bar{1}$	$Pbca$
unit cell	a = 17.6928(9)	a = 27.248(3)	a = 11.3622(5)	a = 9.6380(4)
	b = 14.2748(9)	b = 10.2025(11)	b = 14.0882(5)	b = 19.9218(7)
	c = 8.0082(5)	c = 17.7389(19)	c = 17.6835(7)	c = 25.9126(9)
	α = 90	α = 90	α = 68.245(2)	α = 90
	β = 101.893(3)	β = 108.503(4)	β = 88.857(2)	β = 90
	α = 90	γ = 90	γ = 70.718(2)	γ = 90
V (Å^3)	1979.1(2)	4676.4(8)	2464.57(17)	4975.5
Z	4	4	2	8
D_c (g/cm^3)	1.448	1.477	1.412	1.658
μ (mm^{-1})	0.198	0.573	0.544	1.078
F(000)	904	2168	1100	2496
θ range (deg)	1.85−26.02	2.15−23.25	1.65−26.02	1.57−25.35
refns collected/refns indep	72 839/5158	27 131/3360	36 654/9690	109 274/4556
R_{int}	0.0525	0.0605	0.0475	0.0815
data/restraints/params	3879/0/289	3360/0/327	9690/0/677	4556/0/317
R1, wR2 [$I > 2\sigma(I)$]	0.0472, 0.1173	0.0467, 0.0857	0.0424, 0.0954	0.0549, 0.0952
R1, wR2 (all data)	0.0662, 0.1245	0.1218, 0.1113	0.0638, 0.1053	0.1306, 0.1241
residuals (e Å^{-3})	0.314, −0.422	0.403, −0.688	0.878, −0.673	0.708, −0.960

the calculations were first performed in vacuum, and then in methanol to compare the solvent effect.

To explore the conformational preference of the tetrahydroquinozinoline ligand H_2L^a, the dihedral angle C3−C2−C9−N3 was progressively incremented from 0° to 360°, and the resultant geometries were minimized using PM6, followed by a DFT single point energy calculation. The most stable conformers were further minimized by DFT. A similar protocol was carried out for imine H_2L^i in which case several rotations were made, mainly involving C2−C9, N2−C9a, and C14−C13a bonds.

For palladium(II) and nickel(II) metal complexes, it was considered that the conformation around the metal might not change significantly. Therefore, changes were not made around the metal coordination environment from a defined geometry. A square planar coordination was used for both metal complexes, and an octahedral geometry was also studied for Ni^{II} complexes. A similar protocol was carried out as for ligands H_2L^i and H_2L^a. As a result, four possible conformers were obtained for Pd^{II} complexes and four and seven conformers for square planar and octahedral nickel(II) complexes, respectively (see Supporting Information).

(*E*)-*N*-{2-[(8-Hydroxyquinolin-2-yl)methyleneamino]benzyl}-4-methylbenzene-sulfonamide (H_2L^i). A solution of 8-hydroxyquinoline-2-carboxaldehyde (127 mg, 0.72 mmol) and 2-tosylaminomethylaniline (200 mg, 0.72 mmol) in chloroform (40 mL) was heated under reflux for 1 h. After cooling to room temperature, the resulting pale yellow solution was concentrated in vacuum to give an oily product, which was dissolved in ethanol (20 mL) and stirred for 10 min. This resulted in a pale yellow powder, which was dried in vacuum. Yield = 0.13 g (42%). Mp 126 °C. ^{1}H NMR (500 MHz, DMSO-d_6): δ 10.03 (s, 1H, OH), 8.61 (s, 1H, H-9), 8.42 (d, J = 8.6 Hz, 1H, H-4), 8.11 (d, J = 8.6 Hz, 1H, H-3), 7.93 (t, J = 6.0 Hz, 1H, NH), 7.66 (d, J = 8.2 Hz, 2H, H-16 + H-20), 7.54 (t, J = 7.8 Hz, 1H, H-6), 7.48 (dd, J = 8.1 and 0.9 Hz, 1H, H-5), 7.41 (d, J = 7.5 Hz, 1H, H-13), 7.37 (dt, J = 7.6 and 1.1 Hz, 1H, H-11), 7.29 (d, J = 8.0 Hz, 2H, H-17 + H-19), 7.27 (t, J = 7.5 Hz, 1H, H-12), 7.19 (d, J = 7.7 Hz, 1H, H-10), 7.18 (dd, J = 7.5 and 1.2 Hz, 1H, H-7), 4.18 (d, J = 5.4 Hz, 2H, H-14), 2.32 (s, 3H; H-18). ^{13}C NMR (125 MHz, DMSO-d_6): δ 161.2 (C-9), 154.2 (C-8), 152.5 (C-2), 148.8 (C-9a), 142.9 (C-18a), 138.5 (C-8a), 138.0 (C-15), 137.1 (C-3), 131.9 (C-13a), 129.8 (C-17 + C-19), 129.8 (C-4a), 129.4 (C-13), 129.4 (C-6), 129.1 (C-11), 127.0 (C-12), 126.8 (C-16 + C-20), 118.8 (C-4), 118.1 (C-5), 117.9 (C-10), 112.5 (C-7), 42.4 (C-14), 21.3 (C-18). UV−vis (MeOH, λ in nm, ε in parentheses) 206 (24 782), 248 (19 565), 272 (14 565). FTIR (KBr, cm^{-1}): ν(O−H) 3409(br,m), ν(N−H) 3246(m), ν(C═N_{imi}) 1620(m), ν(C═N_{quin}) 1611(sh, m), $\nu_{as}(SO_2)$ 1336(s), $\nu_s(SO_2)$ 1162(vs). MS (FAB$^+$, MNBA) m/z (%): 432.2 (100) [M + H]$^+$. Anal. Calcd for $C_{24}H_{21}N_3O_3S$: C, 66.8; H, 4.9; N, 9.7; S, 7.3. Found: C, 66.70, H, 4.6, N, 9.7, S, 7.0.

(*rac*)-2-(3-Tosyl-1,2,3,4-tetrahydroquinazolin-2-yl)quinolin-8-ol (H_2L^a). The experimental procedure was the same as for compound H_2L^i, with heating under reflux for 4.5 h. After cooling to room temperature, the reaction mixture was concentrated under reduced pressure to yield an oily product, which was dissolved in ethanol (20 mL) and stirred for 10 min. This resulted in a beige powder, which was dried under vacuum. Yield = 0.27 g (88%). Mp 126 °C. ^{1}H NMR (500 MHz, DMSO-d_6): δ 9.38 (s, 1H, OH), 8.35 (d, J = 8.6 Hz, 1H, H-4), 7.79 (d, J = 8.3 Hz, 2H, H-16 + H-20), 7.62 (d, J = 8.6 Hz, 1H, H-3), 7.44 (t, J = 8.0 Hz, 1H, H-6), 7.38 (dd, J = 8.2 and 1.1 Hz, 1H, H-5), 7.25 (d, J = 8.1 Hz, 2H, H-17 + H-19), 7.11 (dd, J = 7.4 and 1.2 Hz, 1H, H-7), 7.07 (d, J = 3.3 Hz, 1H, NH), 6.88 (dt, J = 7.2 and 1.0 Hz, 1H, H-11), 6.77 (d, J = 7.4 Hz, 1H, H-13), 6.63 (d, J = 8.0 Hz, 1H, H-10), 6.48 (dt, J = 7.4 and 0.9 Hz, 1H, H-12), 6.40 (d, J = 2.8 Hz, 1H, H-9), 4.51 (d, J = 17.1 Hz, 1H, H_{eq}-14), 4.16 (d, J = 17.2 Hz, 1H, H_{ax}-14), 2.30 (s, 3H, H-18). ^{13}C NMR (125 MHz, DMSO-d_6): δ 156.8 (C-2), 152.5 (C-8), 143.2 (C-18a), 141.6 (C-9a), 137.7 (C-4), 137.3 (C-8a), 136.1 (C-15), 129.3 (C-17 + C-19), 128.0 (C-4a), 127.7 (C-6), 127.4 (C-16 + C-20), 127.2 (C-11), 126.4 (C-13), 119.1 (C-3), 117.4 (C-12), 117.1 (C-5), 116.2 (C-13a), 115.6 (C-10), 111.1 (C-7), 67.4 (C-9) 42.4 (C-14), 20.9 (C-18). UV−vis (MeOH, λ in nm, ε in parentheses) 206 (22 173), 248 (23 913), 270 (5434), 298 (2173). FTIR (KBr, cm^{-1}): ν(O−H) 3417(s), ν(N−H) 3398(s), ν(C═N_{quin}) 1611(s), $\nu_{as}(SO_2)$ 1322(s), $\nu_s(SO_2)$ 1157(vs). MS (ESI$^+$, 100 V) m/z (%): 432.2 (100) [M + H]$^+$. Anal. Calcd for $C_{24}H_{21}N_3O_3S$: C, 66.8; H, 4.9; N, 9.7; S, 7.3. Found: C, 66.4; H, 5.0; N, 9.4; S, 7.4.

$Pd(L^i){\cdot}3H_2O$. This compound was prepared by heating under reflux a methanol solution (40 mL) containing H_2L^a and $Pd(OAc)_2{\cdot}4H_2O$ in a 1:1 or 2:1 molar ratio. Alternatively, this reaction could be performed by stirring at room temperature for 16 h or even after only 4 h under reflux if $Pd(OAc)_2$ and the aldehyde were first mixed and then the tosylamine was added to the resulting solution. Filtration of the resulting green suspension yielded a green powder, which was washed

dx.doi.org/10.1021/ic2017038 | Inorg. Chem. 2012, 51, 1278−1293

with diethyl ether and dried under vacuum. Yield = 78%. ^{1}H NMR (500 MHz, DMSO-d_6): δ 8.70 (s, 1H, H-9), 8.45 (d, J = 8.7 Hz, 1H, H-4), 7.80 (d, J = 8.8 Hz, 1H, H-3), 7.78 (d, J = 8.3 Hz, 2H, H-16 + H-20), 7.63 (d, J = 8.0 Hz, 1H, H-10), 7.46 (t, J = 8.0 Hz, 1H, H-6), 7.42 (dt, J = 7.8 and 1.5 Hz, 1H, H-11), 7.34 (t, J = 7.4 Hz, 1H, H-12), 7.30 (dd, J = 7.4 and 1.2 Hz, 1H, H-13), 7.13 (d, J = 8.0 Hz, 2H, H-17 + H-19), 6.93 (d, J = 8.1 Hz, 1H, H-5), 6.59 (d, J = 8.0 Hz, 1H, H-7), 4.24 (s, 2H, H-14), 2.36 (s, 3H, H-18). ^{13}C NMR (125 MHz, DMSO-d_6): δ 174.1 (C-8), 168.2 (C-9), 148.2 (C-2), 144.2 (C-8a), 142.6 (C-15), 140.4 (C-18a + C-9a), 138.2 (C-4), 137.3 (C-13a), 136.8 (C-6), 132.0 (C-4a), 131.3 (C-13), 130.7 (C-12), 129.3 (C-11), 129.0 (C-17 + C-19), 126.9 (C-16 + C-20), 122.6 (C-3), 119.9 (C-10), 114.9 (C-7), 111.7 (C-5), 49.8 (C-14), 21.3 (C-18). FTIR (KBr, cm^{-1}): ν(O−H) 3442(b,m), ν(C═N$_{imi}$) 1586(s), ν(C═N$_{quin}$) 1563(m), ν_{as}(SO$_2$) 1336(s), ν_s(SO$_2$) 1142(vs). MS (FAB$^+$) m/z (%): 536.0 (100) [M$^+$ − 3H$_2$O]. Anal. Calcd for $C_{24}H_{19}N_3O_3PdS{\cdot}3H_2O$: C, 48.8; H, 4.2; N, 7.1; S, 5.4. Found: C, 48.2; H, 3.9; N, 7.0; S, 5.2.

Pd(HL^i)$_2$·MeOH. This compound was obtained from a methanol solution (40 mL) containing H_2L^a and Pd(OAc)$_2$·4H$_2$O in a 1:2 molar ratio under reflux for 2 h. During the reaction the color of the solution changed from the initial green, which is due to the formation of Pd(L^i), to the final maroon. Filtration of the resulting suspension yielded a maroon powder, which was washed with diethyl ether and dried under vacuum. Yield: 57%. ^{1}H NMR (500 MHz, DMSO-d_6): δ 9.33 (s, 1H, H-9), 8.16 (d, J = 8.6 Hz, 1H, H-4), 7.90 (t, J = 6.1 Hz, 1H, NH), 7.74 (d, J = 8.5 Hz, 1H, H-3), 7.70 (d, J = 8.1 Hz, 2H, H-16 + H-20), 7.42 (d, J = 7.4 Hz, 1H, H-13), 7.37 (d, J = 8.1 Hz, 2H, H-17 + H-19), 7.27 (d, J = 7.3 Hz, 1H, H-10), 7.25 (t, J = 7.4 Hz, 1H, H-12), 7.20 (t, J = 7.4 Hz, 1H, H-11), 7.14 (t, J = 7.6 Hz, 1H, H-6), 6.84 (d, J = 7.8 Hz, 1H, H-5), 6.49 (d, J = 7.8 Hz, 1H, H-7), 4.16 (d, J = 6.0 Hz, 2H, H-14), 2.37 (s, 3H, H-18). ^{13}C NMR (125 MHz, DMSO-d_6): δ 158.6 (C-9), 139.5 (C-4), 130.7 (C-6), 129.8 (C-17 + C-19), 129.3 (C-13), 127.8 (C-11), 127.8 (C-12), 126.8 (C-16 + C-20), 120.0 (C-3), 118.5 (C-10), 114.1 (C-7), 112.7 (C-5), 42.4 (C-14), 21.4 (C-18). FTIR (KBr, cm^{-1}): ν(O−H) 3430(b,m), ν(N−H) 3289(m), ν(C═N$_{quin}$) 1598(m), ν(C═N$_{imi}$) 1557(s), ν_{as}(SO$_2$) 1328(s), ν_s(SO$_2$) 1161(vs). MS (MALDI$^+$-TOF) m/z (%): 1005.1 (9) [M − MeOH + K]$^+$. Anal. Calcd for $C_{48}H_{40}N_6O_6PdS_2{\cdot}$MeOH: C, 58.9; H, 4.4; N, 8.4; S, 6.4. Found: C, 58.9; H, 4.0; N, 8.5; S, 6.4.

Ni(L^i)·MeOH. This complex was obtained by stirring a methanol solution (40 mL) containing 0.1 g (0.231 mmol) of H_2L^i (or H_2L^a) and 0.057 g of Ni(OAc)$_2$·4H$_2$O (0.231 mmol) at room temperature for around 5 min. Concentration under reduced pressure of the resulting brown solution yielded an oily product, which was stirred with diethyl ether (20 mL) for 10 min. This gave a brown powder, which was filtered off and dried in vacuum. Yield: 0.053 g (44%). UV−vis (MeOH, nm) λ 196, 277. MS (FAB, positive) m/z (%): 488.1 (100) [M − MeOH + H]$^+$. FTIR (KBr, cm^{-1}): ν(O−H) 3420 (b,m), ν(C═N$_{imi}$) 1595 (vs), ν_{as}(SO$_2$) 1344(s), ν_s(SO$_2$) 1162(vs). Anal. Calcd for $C_{24}H_{19}N_3NiO_3S{\cdot}$MeOH: C, 57.7; H, 4.5; N, 8.1; S, 6.2. Found: C, 57.9; H, 5.0; N, 8.4; S, 6.1.

Ni(HL^a)$_2$·4MeOH. This complex was obtained by stirring a methanol solution (40 mL) containing H_2L^a (or H_2L^i) and Ni(OAc)$_2$·4H$_2$O in 1:2, 2:1, 3:2, or 1:1 molar ratios at room temperature over a 14 h period or under reflux for around 1 h. Concentration under reduced pressure of the brown solution yielded an oily product, which was dissolved in diethyl ether (20 mL) and stirred for 10 min. This gave an orange crystalline powder, which was filtered off and dried in vacuum. Single crystals of Ni(HL^a)$_2$·4MeOH and Ni(HL^a)$_2$·2HOAc were obtained from the mother liquor. Yield: 78%. UV−vis (MeOH, nm, ε in parentheses) λ 210 (51 142), 270 (42 285), 380 (3428) [ν_2 $^3T_{1\,g}(F) \leftarrow {}^3A_{2\,g}(F)$], 510 (400) [$\nu_3$ $^3T_{1\,g}(P) \leftarrow {}^3A_{2\,g}(F)$]. MS (FAB, positive) m/z (%): 919.0 (80) [M$^+$ − 4MeOH]. FTIR (KBr, cm^{-1}): ν(O−H) 3415(b,m), ν(N−H) 3303(m), ν(C═N$_{quin}$) 1598(m), ν_{as}(SO$_2$) 1347(s), ν_s(SO$_2$) 1163(vs). Anal. Calcd for $C_{48}H_{40}N_6NiO_6S_2{\cdot}$4MeOH: C, 59.6; H, 5.4; N, 8.0; S, 6.1; S, 7.3. Found: C, 59.9; H, 5.1; N, 8.4; S, 6.1.

■ ASSOCIATED CONTENT

Ⓢ Supporting Information

CIF data. Energy details of the most stable conformers of compounds H_2L^i and H_2L^a, square planar Pd^{II} and Ni^{II} complexes, as well as octahedral Ni^{II} complexes. Representative NMR bidimensional spectra of compounds H_2L^i, H_2L^a and Pd(HL^i)$_2$ as well as ^{1}H NMR spectrum of Pd(HL^a)$_2$. IR and UV−vis spectra of Pd(HL^i)$_2$·MeOH, Ni(HL^a)$_2$·4MeOH, Pd(L^i)·3H$_2$O, and Ni(L^i)·MeOH. Energy details of the reaction intermediates and transition states. This material is available free of charge via the Internet at http://pubs.acs.org.

■ AUTHOR INFORMATION

Corresponding Author

*E-mail: jesus.sanmartin@usc.es. Fax: +34 981 528073.

■ ACKNOWLEDGMENTS

Financial support from the Ministerio de Ciencia e Innovación (CTQ2010-19191 to J.S.-M. and SAF2010-15076 to C.G.-B.) and the Xunta de Galicia (10PXIB2200122PR and GRC2010/12 to C.G.-B.) is gratefully acknowledged. We are also grateful to the Centro de Supercomputación de Galicia (CESGA) for the use of the Finis Terrae computer.

■ REFERENCES

(1) Boca, M.; Baran, P.; Boca, R.; Fuess, H.; Kickelbick, G.; Linert, W.; Renz, F.; Svoboda, I. *Inorg. Chem.* **2000**, *39*, 3205−3212.
(2) Zeyrek, C. T.; Elmali, A.; Elerman, Y. *Z. Naturforsch.* **2005**, *60b*, 520−526.
(3) (a) Bera, M.; Mukhopadhyay, U.; Ray, D. *Inorg. Chim. Acta* **2005**, *358*, 437−443. (b) Nanda, P. K.; Mandal, D.; Ray, D. *Polyhedron* **2006**, *25*, 702−710.
(4) Emam, S. A.; McArdle, P.; McManus, J.; Mahon, M. *Polyhedron* **2008**, *27*, 2379−2385.
(5) (a) Bermejo, M. R.; Sousa, A.; Fondo, M.; Helliwell, M. *New J. Chem.* **2000**, *24*, 33−38. (b) Sousa, A.; Bermejo, M. R.; Fondo, M.; García-Deibe, A.; Sousa-Pedrares, A.; Piro, O. *New J. Chem.* **2001**, *25*, 647−654.
(6) Bréfuel, N.; Lepetit, C.; Shova, S.; Dahan, F.; Tuchagues, J.-P. *Inorg. Chem.* **2005**, *44*, 8916−8928.
(7) Çolak, A. T.; Taş, M.; İrez, G.; Yeşilel, O. Z.; Büyükgüngör, O. *Z. Anorg. Allg. Chem.* **2007**, *633*, 504−508.
(8) Mutlu, H.; İrez, G.; Turk, J. *Chemistry* **2008**, *32*, 731−741.
(9) (a) Vázquez, M.; Bermejo, M. R.; Sanmartín, J.; García-Deibe, A. M.; Lodeiro, C.; Mahia, J. *J. Chem. Soc., Dalton Trans.* **2002**, 870−877. (b) Fondo, M.; Ocampo, N.; García-Deibe, A. M.; Sanmartín, J. *Inorg. Chem.* **2009**, *48*, 4971−4979.
(10) (a) García-Santos, I.; Sanmartín, J.; García-Deibe, A. M.; Fondo, M.; Gómez, E. *Inorg. Chim. Acta* **2010**, *363*, 193−198. (b) García-Santos, I.; Sanmartín, J.; García-Deibe, A. M.; Fondo, M.; Gómez, E. *Polyhedron* **2009**, *28*, 3055−3059.
(11) Parr, R. G.; Pearson, R. G. *J. Am. Chem. Soc.* **1983**, *105*, 7512−7516.
(12) For example, see: Karayannis, N. M.; Pytlewsky, L. L.; Mikulsky, C. M. *Coord. Chem. Rev.* **1973**, *11*, 93−159.
(13) For example, see: Cooke, M. W.; Chartrand, D.; Hanan, G. S. *Coord. Chem. Rev.* **2008**, *252*, 903−921.
(14) Shannon, R. D. *Acta Crystallogr.* **1976**, *A32*, 751−767.
(15) Sanmartín, J.; Novio, F.; García-Deibe, A. M.; Fondo, M.; Bermejo, M. R. *New J. Chem.* **2007**, *31*, 1605−1612.
(16) Baldwin, J. E. *J. Chem. Soc., Chem. Commun.* **1976**, 734−736.
(17) Frisch, M. J.; Trucks, G. W.; Schlegel, H. B.; Scuseria, G. E.; Robb, M. A.; Cheeseman, J. R.; Scalmani, G.; Barone, V.; Mennucci, B.; Petersson, G. A.; Nakatsuji, H.; Caricato, M.; Li, X.; Hratchian, H. P.; Izmaylov, A. F.; Bloino, J.; Zheng, G.; Sonnenberg, J. L.; Hada, M.; Ehara, M.; Toyota, K.; Fukuda, R.; Hasegawa, J.; Ishida, M.;

Nakajima, T.; Honda, Y.; Kitao, O.; Nakai, H.; Vreven, T.; Montgomery, J. A., Jr.; Peralta, J. E.; Ogliaro, F.; Bearpark, M.; Heyd, J. J.; Brothers, E.; Kudin, K. N.; Staroverov, V. N.; Kobayashi, R.; Normand, J.; Raghavachari, K.; Rendell, A.; Burant, J. C.; Iyengar, S. S.; Tomasi, J.; Cossi, M.; Rega, N.; Millam, N. J.; Klene, M.; Knox, J. E.; Cross, J. B.; Bakken, V.; Adamo, C.; Jaramillo, J.; Gomperts, R.; Stratmann, R. E.; Yazyev, O.; Austin, A. J.; Cammi, R.; Pomelli, C.; Ochterski, J. W.; Martin, R. L.; Morokuma, K.; Zakrzewski, V. G.; Voth, G. A.; Salvador, P.; Dannenberg, J. J.; Dapprich, S.; Daniels, A. D.; Farkas, Ö.; Foresman, J. B.; Ortiz, J. V.; Cioslowski, J.; Fox, D. J. *Gaussian 09, Revision A.2*; Gaussian, Inc.: Wallingford CT, 2009.

(18) Zhao, Y.; Truhlar, D. G. *Theor. Chem. Acc.* **2008**, *120*, 215−241.

(19) Zhao, Y.; Truhlar, D. G. *Acc. Chem. Res.* **2008**, *41*, 157−167.

(20) Tomasi, J.; Mennucci, B.; Cammi, R. *Chem. Rev.* **2005**, *105*, 2999−3094.

(21) (a) Ochs, C.; Hahn, F. E.; Lugger, T. *Eur. J. Inorg. Chem.* **2001**, 1279−1285. (b) Ochs, C.; Hahn, F. E.; Frohlich, R. *Chem.—Eur. J.* **2000**, *6*, 2193−2199.

(22) (a) Otter, C. A.; Couchman, S. M.; Jeffery, J. C.; Mann, K. L. V.; Psillakis, E.; Ward, M. D. *Inorg. Chim. Acta* **1998**, *278*, 178−184. (b) Cabaleiro, S.; Castro, J.; Vázquez-Pérez, E.; García-Vázquez, J. A.; Romero, J.; Sousa, A. *Polyhedron* **1999**, *18*, 1669−1674. (c) Mahía, J.; Maestro, M.; Vázquez, M.; Bermejo, M. R.; Sanmartín, J.; Maneiro, M. *Acta Crystallogr.* **1999**, *C55*, 1545−1547. (d) Vázquez, M.; Bermejo, M. R.; Sanmartín, J.; García-Deibe, A. M.; Lodeiro, C.; Mahía, J. *J. Chem. Soc., Dalton Trans.* **2002**, 870−877. (e) Bermejo, M. R.; Sanmartín, J.; García-Deibe, A. M.; Fondo, M.; Novio, F.; Navarro, D. *Inorg. Chim. Acta* **2003**, *347*, 53−60. (f) Garnovskii, A.; Guedes da Silva, M. F. C.; Koplovich, M. N.; Garnovskii, A. D.; Frausto da Silva, J. J. R.; Pombeiro, A. J. L. *Polyhedron* **2003**, *22*, 1335−1340. (g) Sanmartín, J.; García-Deibe, A. M.; Fondo, M.; Novio, F.; Ocampo, N.; Bermejo, M. R. *Inorg. Chim. Acta* **2006**, *359*, 3156−3166.

(23) (a) Roychowdhury, P.; Das, B. N.; Basak, B. S. *Acta Crystallogr.* **1978**, *B34*, 1047−1048. (b) Banerjee, T.; Saha, N. N. *Acta Crystallogr.* **1986**, *C42*, 1408−1411. (c) Ali, M. A.; Mirza, A. H.; Haniti, M.; Hamid, S. A.; Bernhardt, P. V. *Polyhedron* **2005**, *24*, 383−390.

(24) (a) Lennon, D.; Freer, A. A.; Winfield, J. M.; Landon, P.; Reid, N. *Green Chem.* **2002**, *4*, 181−187. (b) Wang, Z.-G.; Wang, R.; Zhang, Y.; Zhi, F.; Yang, Y.-L. *Acta Crystallogr.* **2009**, *E65*, o550.

(25) (a) Jeffrey, G. A. *An Introduction to Hydrogen Bonding*; Oxford University Press: Oxford, U.K., 1997. (b) Steiner, T. *Angew. Chem., Int. Ed.* **2002**, *41*, 48−76.

(26) (a) *SADABS−Bruker AXS Area Detector Scaling and Absorption Correction, Version 2008/1*; University of Göttingen: Göttingen, Germany, 2008. (b) Blesing, R. H. *Acta Crystallogr.* **1995**, *A51*, 33−38.

(27) Burla, M. C.; Caliandro, R.; Camalli, M.; Carrozzini, B.; Cascarano, G. L.; De Caro, L.; Giacovazzo, C.; Polidori, G.; Spagna, R. *J. Appl. Crystallogr.* **2005**, *38*, 381−388.

(28) Sheldrick, G. M. SHELX97. *Acta Crystallogr.* **2008**, *A64*, 112−122.

(29) (a) Allen, F. H. *Acta Crystallogr.* **2002**, *B58*, 380−388. (b) Bruno, I. J.; Cole, J. C.; Edginton, P. R.; Kessler, M. C.; Macrae, F.; McCabe, P.; Pearson, J.; Taylor, R. *Acta Crystallogr.* **2002**, *B58*, 389−397.

(30) For examples, see: (a) Zimmer, M.; Schulte, G.; Luo, X.-L.; Crabtree, R. H. *Angew. Chem., Int. Ed.* **1991**, *30*, 193−194. (b) Ohta, H.; Harada, K.; Irie, K.; Kashino, S.; Kambe, T.; Sakane, G.; Shibahara, T.; Takamizawa, S.; Mori, W.; Nonoyama, M.; Hirotsu, M.; Kojima, M. *Chem. Lett.* **2001**, 842−843. (c) Okabe, N.; Muranishi, Y. *Acta Crystallogr.* **2002**, *C58*, m475−m477. (d) Cui, X.; Calhorda, M. J.; Costa, P. J.; Delgado, R.; Drewand, M. G. B.; Felix, V. *Helv. Chim. Acta* **2004**, *87*, 2613−2628. (e) You, Z.-L.; Zhu, H.-L.; Liu, W.-S. *Acta Crystallogr.* **2004**, *E60*, m805−m807. (f) Fondo, M.; García-Deibe, A. M.; Ocampo, N.; Sanmartín, J.; Bermejo, M. R.; Llamas-Saiz, A. L. *Dalton Trans.* **2006**, *45*, 4260−4270.